Detection of organic carbon in Mars-analog paleosols with thermal and evolved gas analysis

Adrian P. Broz* [1,] Joanna Clark[2], Brad Sutter[3], Doug W. Ming[4], Briony Horgan[5], Paul Douglas Archer Jr.[3] and Lucas C.R. Silva[6,7]

[1]Department of Earth Sciences, University of Oregon, Eugene, OR 97405

[2]Geocontrols Systems – Jacobs JETS Contract, NASA Johnson Space Center, Houston, TX, 77058

[3]Jacobs JETS Contract, NASA Johnson Space Center, Houston, TX 77058

[4]NASA Johnson Space Center, Houston, TX, 77058

[5]Department of Earth, Atmospheric and Planetary Science, Purdue University, IN, 47907

[6]Environmental Studies Program, Department of Geography, University of Oregon, Eugene, OR 97405

[7]Institute of Ecology and Evolution, University of Oregon, Eugene, OR 97405

*Corresponding author, abroz@uoregon.edu

Key points

- Trace amounts of organic carbon (OC) and organic fragments in Mars-analog paleosols were detected with thermal and evolved gas analysis
- The near-surface horizons of 33-million-year-old paleosols had significantly higher OC content relative to deeper layers
- Radiocarbon dates of approximately 6-14 thousand years were consistent with small amounts of modern carbon in paleosol samples

This paper is a non-peer reviewed preprint submitted to EarthArXiv.

It is currently under review in JGR: Planets (Revision 1 Submitted April 19, 2022)

Abstract

Ancient, buried soils, or paleosols, may have been preserved in the geological record on Mars, and are considered high-priority targets for biosignature investigation. Studies of paleosols on Earth that are similar in composition to putative martian paleosols can provide a reference frame for constraining their organic preservation potential on Mars. However, terrestrial paleosols typically preserve only trace amounts of organic carbon, and determining what carbon is original is complicated by diagenesis and additions of modern carbon. The objectives of this study were a) to determine whether organic carbon in Mars-analog paleosols can be detected with thermal and evolved gas analysis, and b) constrain the age of organic carbon using radiocarbon (^{14}C) dating. Oligocene (33 Ma) paleosols from Oregon were examined with an instrument similar to the Sample Analysis at Mars Evolved Gas Analysis (SAM-EGA) instrument onboard the Mars Science Laboratory *Curiosity* rover. Trace amounts of organic carbon and fragments of organic molecules were observed in all samples. Total organic carbon (TOC) ranged from 0.002 - 0.032 ± 0.006 wt. %. The near-surface horizons of paleosols had significantly higher TOC relative to subsurface layers. Radiocarbon dating of four samples revealed an organic carbon age of ~6,200 – 14,500 years before present and a fraction modern ranging from 0.16-0.46. Modeled abundances of modern carbon in bulk samples ranged from 0.41 – 3.1 % ± 0.11%, which were consistent with additions of small amounts of modern organic carbon. This work demonstrates that martian paleosols are a potential high priority location for *in-situ* biosignature investigation.

Plain language summary

Ancient, buried soils, or paleosols, may have been preserved in the geological record on Mars. On Earth, paleosols that are billions of years old contain signs of ancient life (biosignatures) and therefore paleosols on Mars are considered high-priority locations for biosignature investigation. One way to determine the biosignature preservation potential of possible martian paleosols is to examine organic carbon preservation in paleosols from Earth that resemble martian paleosols. The objectives of this work were to determine if carbon in Mars-analog paleosols can be detected by an instrument configured to operate like the Sample Analysis at Mars (SAM) Evolved Gas Analyzer (SAM-EGA) onboard *Curiosity* rover, and to use radiocarbon dating to determine if samples contain modern carbon. Trace amounts of organic carbon and fragments of organic molecules were observed. Like modern soils, the near-surface horizons of all paleosols had significantly higher amounts of carbon relative to subsurface layers. Radiocarbon dating revealed an organic carbon age of ~6,200 – 14,500 years before present. Application of an isotopic mixing model suggested these dates could be explained by slight additions of modern carbon to ancient samples. These results demonstrate that putative martian paleosols are a potential high priority location for *in-situ* biosignature investigation.

Introduction

Paleosols are ancient, buried soils that are commonly lithified into sedimentary rocks. Terrestrial paleosols are a geological record of the atmospheric composition, climate, topography and organisms present before soil burial (Retallack, 2019). On Mars, paleosols, also known as weathering profiles, may have formed in sediments such as basaltic sand or volcanic ash that were subject to subaerial weathering by surface waters (Retallack, 2014; Amundson, 2018; Liu et al., 2021b; Ye and Michalski, 2021) and were subsequently buried and preserved in the geological record. Orbital remote sensing of the global martian surface has detected dioctahedral clay minerals within Noachian (4.1-3.7 Ga) layered sedimentary rocks, which are consistent with precipitation-driven pedogenic weathering of mafic sediments (Carter et al., 2015; Bishop et al., 2018b; Loizeau et al., 2018). Noachian sedimentary rocks with spectral signatures of subaerial weathering have been detected in thousands of locations across the surface of Mars (Bishop et al., 2018b). One hypothesis is that these deposits are paleosols (Carter et al., 2015), which are the common products of pedogenic alteration followed by burial. Mounting evidence of global-scale aqueous alteration of the Martian surface during the Noachian (Carter et al., 2015; Liu et al., 2021a) suggests that pedogenesis could have been a critical process early in the planet's history. As such, paleosols have been recently named a high priority location for biosignature investigation (Bishop et al., 2018a) and Mars Sample Return (Beaty et al., 2019), but the biosignature preservation potential of paleosols with Mars-like mineralogy remains poorly constrained (Horgan, 2016).

On Earth, soils are highly habitable environments. Modern soils are teeming with microbial biomass, often averaging 10^{10}–10^{11} bacterial cells and 10^{3} and 10^{4} species per gram of soil (Raynaud and Nunan, 2014). Modern soils also contain more organic carbon than global vegetation and the atmosphere combined (Lehmann and Kleber, 2015; Dynarski et al., 2020). Similarly, Earth's oldest soils also appear to have been highly habitable environments. Many Precambrian (> 541 Ma) paleosols contain organic carbon and other chemical biosignatures that are thought to be remnants of surface biomass (Matthewman et al., 2012; Kremer et al., 2017; Liivamägi et al., 2018; Broz, 2020). Furthermore, Archean (> 2 Ga) paleosols contain filamentous organic carbon and organo-mineral complexes possibly derived from cyanobacterial mats on the soil surface (Rye and Holland, 2000; Watanabe et al., 2000).

Many terrestrial paleosols preserve only trace amounts of organic carbon, especially compared to modern soils, marine shales, and lacustrine rocks (Retallack, 2019). Organic carbon losses during diagenesis can reduce the organic carbon content of paleosols by up to two orders of magnitude relative to their modern soil counterparts (Broz, 2020). Severe losses of organic carbon are most common in paleosols that originally formed under oxidizing, well-drained conditions (Retallack and Mao, 2019). In general, oxidized paleosols typically contain only low amounts (< 0.1 wt. %) of organic carbon (Broz, 2020). Diagenetic losses of organic carbon in oxidized terrestrial paleosols poses major challenges for

detection of chemical and isotopic biosignatures preserved within the organic matter fraction. However, this is not the case for all paleosols. Those that originally formed under reducing conditions, such as Permian (~250 Ma) Histosols (poorly drained organic soils), preserve organic carbon with abundances > 25 wt. % (Retallack and Krull, 1999), implying that redox state before burial may provide a first-order control on the preservation of organic carbon in ancient soils (Krull and Retallack, 2000).

An additional concern for the study of terrestrial paleosol organic matter is that diagenetic alterations ranging from groundwater alteration to precipitation-driven leaching of dissolved organic carbon can result in the addition of exogenous (e.g., allochthonous) organic molecules, so caution is necessary for interpreting whether the organic fraction has indeed been "preserved" over geological time scales. In other words, terrestrial paleosols can be contaminated by organic molecules that were not original to the soil, thereby complicating efforts to interpret their biosignature preservation potential.

One way to constrain the biosignature preservation potential of putative paleosols on Mars is to examine the organic fraction of paleosols from Earth that share compositional and morphological similarities to layered sedimentary rocks on Mars. Examination of oxidized paleosols with Mars-like mineralogy can help determine if low amounts of organic molecules within natural pedogenic mineral matrices can be detected with Mars flight-analog instruments. Furthermore, cosmogenic nuclide dating of these analog paleosols can also identify potential diagenetic additions of organic carbon.

This study builds on and combines previous results from an established Mars-analog paleosol sequence (Broz et al., 2021, 2022). The focus here is to determine if organic molecules in oxidized paleosols are detectable with Mars flight-analog instrumentation, and to determine if there have been post-depositional additions of modern organic carbon. The objectives of this study were a) to determine whether organic carbon in ~33-million-year-old Mars-analog paleosols can be detected with thermal and evolved gas analysis, and b) constrain the age of organic carbon using radiocarbon (^{14}C) dating.

1.1 Paleosols at John Day Fossil Beds National Monument in eastern Oregon, USA

Eocene and Oligocene (42 to 28 Ma) sedimentary rocks at John Day Fossil Beds National Monument in eastern Oregon are a thick sequence of volcaniclastic paleosols, which altogether spans over 400 meters of vertical stratigraphy (Bestland, 1997; Retallack et al., 2000; Horgan et al., 2012; Smith et al., 2018a). The paleosol sequence contains over 500 clay-rich (30-95 wt. %) paleosols formed over ~15 Myr through the Eocene-Oligocene boundary (Figure 1) (Retallack et al., 2000; Horgan et al., 2018). Each of the individual profiles formed from pedogenic alteration of andesitic to rhyodacitic volcanic ash and/or tuff, followed by rapid burial via emplacement of an additional layer of tephra onto the soil surface. This process of soil formation and burial repeated for nearly 15 million years, and as such, the paleosol sequence provides a unique record of Cenozoic climate change in eastern Oregon (Fremd, 1996).

Changes in mineralogy throughout the paleosol sequence reflect the Eocene-Oligocene cooling and drying of the climate (Bestland, 2002; Retallack et al., 2004).

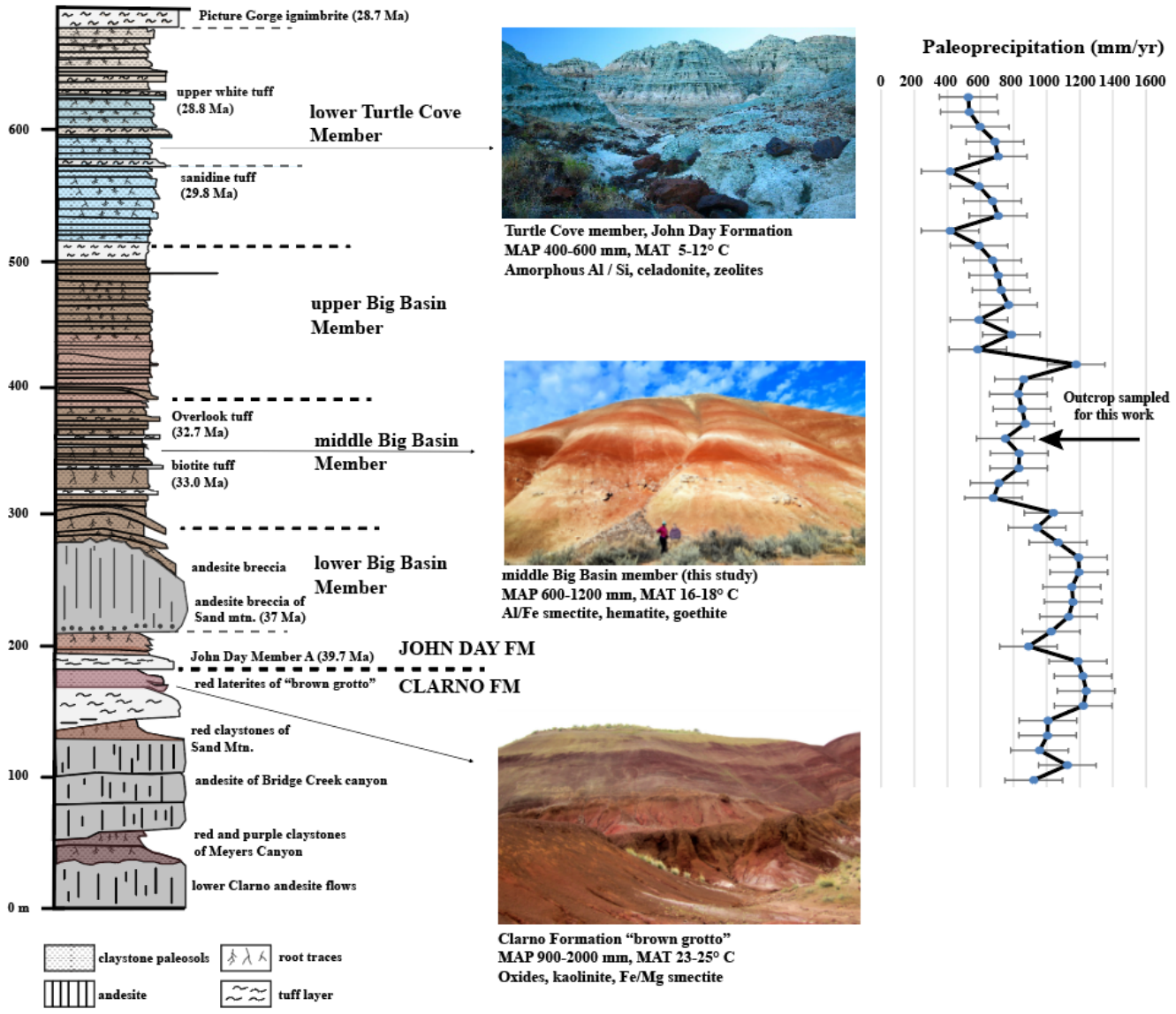

Figure 1. A sequence of Eocene and Oligocene (42-28 Ma) volcaniclastic paleosols in the Clarno and John Day Formations, John Day Fossil Beds National Monument (after Bestland (1997) **and** Sheldon et al. (2002)**.** Declining precipitation through the Eocene/Oligocene boundary is inferred from the mineralogy of paleosols from the Clarno and John Day Formations. Paleoprecipitation estimates are from Sheldon et al. (2002) who used an equation relating molecular weathering ratios (Bases/alumina [$CaO + MgO + Na_2O + K_2O$ / Al_2O_3] to mean annual precipitation from a database of modern U.S soils (r=0.79, standard error = 179 mm). The stratigraphic level of paleosols analyzed in this work are indicated (black arrow, far right).

The Eocene (42-39 Ma) Clarno Formation represents the lowest and oldest unit of the Oregon paleosol sequence. The basal Clarno Formation is characterized by andesite flows interspaced with

153 severely weathered paleosols with accumulations of kaolinite, Fe/Mg smectite and oxides (Oxisols and
154 Ultisols in US soil taxonomy), which indicate tropical weathering conditions in the middle to late Eocene
155 (Retallack et al., 2000). A particularly striking exposure of the late Eocene Clarno Formation at the
156 "Brown Grotto" area of the Painted Hills is characterized by thick (~2-6 meter), repeated profiles of
157 deeply weathered lateritic paleosols (Figure 1, bottom) that are similar to modern soils from Southern
158 Mexico and Central America in climates that are subtropical and humid (Retallack et al., 2000).
159 Stratigraphically above the Clarno Formation, the early Oligocene (~33 Ma) Big Basin Member of the
160 John Day Formation is characterized by less intensely weathered paleosols (Alfisols and Inceptisols) that
161 are rich in Al and Fe smectites such as nontronite and montmorillonite (Figure 1, middle). This middle
162 unit represents a dramatic cooling and drying of the climate through the Eocene-Oligocene boundary.
163 Overlying this unit of the paleosol sequence is the mid-late Oligocene (~28 Ma) Turtle Cove Member of
164 the John Day Formation (Figure 1, top). The brown, green and celadon-colored paleosols of this unit are
165 minimally weathered Aridisols (desert soils) and Andisols (amorphous-rich volcanic soils). Paleosols in
166 this unit are characterized by accumulations of amorphous and nanocrystalline materials (e.g., allophane
167 and imogolite), pedogenic calcite, and diagenetic celadonite (Horgan et al., 2012). There is a dramatic
168 reduction in smectite content and absence of kaolinite, which is consistent with weathering under a semi-
169 arid to arid climate regime (Bestland, 2002). Finally, the entire paleosol sequence is capped by
170 approximately 300 vertical meters of flood basalts from the Miocene (~16 Ma) Columbia River Basalt
171 Group. Based on these mineralogical transitions, the Eocene paleosols with accumulations of kaolinite
172 and oxides appear to reflect a subtropical and humid climate, while accumulations of nanophase
173 aluminosilicates and amorphous phases in overlying paleosols indicate stepwise and cooling and drying
174 during the late Oligocene (Retallack et al., 2000).
175
176 **1.2 Pedogenic weathering on early Mars and comparisons to terrestrial paleosols**
177 From a global perspective, orbital remote sensing from Observatoire pour la Minéralogie, l'Eau,
178 les Glaces, et l'Activité (OMEGA) and the Compact Reconnaissance Spectrometer at Mars (CRISM)
179 instrument onboard the Mars Reconnaissance Orbiter provide the most compelling evidence of extensive
180 pedogenic-like alteration across the surface of Mars. Potential weathering sequences have been detected
181 in hundreds of locations across Noachian terrains, wherever these ancient rocks are not obscured by dust,
182 sand, or overlying strata (Carter et al., 2015; Loizeau et al., 2018). OMEGA and CRISM have collectively
183 gathered visible and near-infrared (VNIR) reflectance spectra of sedimentary deposits at Mawrth Vallis,
184 Oxia Planum, Nili Fossae and other altered Noachian terrains. (Horgan et al., 2012, 2018; Hays et al.,
185 2017; Smith et al., 2018b; Poulet et al., 2020). Spectral refinements for CRISM images (e.g., Viviano-
186 Beck et al., 2014) now allow for identification of smaller-scale hydrated mineral deposits at Mawrth

Vallis that facilitate a detailed reconstruction of possible geochemical environments on early Mars (Bishop et al., 2020). Some of these deposits, such as layered outcrops at Mawrth Vallis, have spectral and stratigraphic similarities to terrestrial paleosol sequences (Horgan et al., 2012; Broz et al., 2022).

Terrestrial paleosols: Mineralogy and diagenesis

The present study focuses on three paleosol profiles from the early Oligocene (33 Ma) Big Basin Member of the John Day Formation (Figure 1, middle). A detailed analysis of mineralogy and diagenetic alteration of these samples was previously performed (Broz et al., 2022). X-ray diffraction, evolved gas analysis and visible-near-infrared spectroscopy revealed high abundances (> 80 wt. %) of montmorillonite and nontronite with lesser amounts of hematite, zeolites, gypsum, and hydrated silica (Tables S4-S6). Diagenetic alterations previously observed in these samples included a) "burial gleization" of near-surface horizons, which is attributed to microbial reduction of Fe^{3+} in near-surface horizons of paleosols resulting from anaerobic decay of organic matter; b) dehydration of ferrous oxyhydroxides (goethite) to form fine-grained hematite; c) zeolitization to form clinoptilolite, possibly resulting from diagenetic recrystallization of a poorly crystalline smectite; and d) significant mechanical compaction to approximately 70% of the original soil thickness (Retallack et al., 2000).

Previously, there was no effort to examine the organic component of these paleosols, and the resulting influence of diagenesis on the organic fraction of Mars-analog paleosols is poorly understood. Examination of terrestrial paleosols with Mars flight-analog instruments such as evolved gas analysis allows for a detailed characterization of the organic fraction (discussed below). This can help ascertain if diagenesis has resulted in severe losses of the organic carbon in Mars-analog paleosols and determine if organic carbon that remains is detectable with analytical techniques relevant to Mars exploration.

1.3 Sample Analysis at Mars (SAM) instrument onboard *Curiosity* Mars Rover

The overall goal of the SAM instrument is to assess the potential for past habitability by characterizing the martian chemical and isotopic composition of the atmosphere and volatile-bearing surface materials (Mahaffy et al., 2012). The SAM instrument is integral in providing an understanding of organic materials and phases undetectable by CheMin (e.g., amorphous phases, low abundance phases). SAM heats scooped or drilled rock samples from ~30 – 870° C at 35° C min^{-1}. Evolved gases produced from the thermal decomposition of volatile-bearing phases are analyzed by a quadrupole mass spectrometer (QMS), gas chromatograph columns for GCMS, or a tunable laser spectrometer (TLS) (Mahaffy et al., 2012). In evolved gas analysis (SAM-EGA) mode, SAM detects bulk gas evolution, whereas in gas chromatography-mass spectroscopy (SAM-GCMS) mode, SAM performs molecular separation and identification of organic molecules (Mahaffy et al., 2012; Eigenbrode et al., 2018). This

study focused on SAM-EGA, so SAM-GCMS will not be further discussed. A comprehensive discussion on how organic molecules are detected with SAM- GCMS mode can be found in Mahaffy et al. (2012) and Szopa et al. (2020).

Evolved gases and their release temperatures detected by SAM-EGA provide constraints on the mineralogy and organic content of samples in Gale Crater (Archer et al., 2014; Ming et al., 2014; Freissinet et al., 2015; Eigenbrode et al., 2018). The thermal decomposition of solid samples during SAM-EGA occurs during ramped heating, which releases volatile gases including CO_2, CO, hydrocarbons, and organic fragments (i.e., CH_2, CH_3, C_2H_2 and others) that are detected by the QMS. The intensity (relative abundance) of volatile release is plotted as a function of the release temperature, generating a time and temperature series of data for each volatile gas release. The volatile release peak temperature during sample decomposition depends on the thermodynamics of the reaction and can be used to constrain the composition of minerals and organic carbon in the sample (Archer et al., 2014), as well as to identify possible associations between minerals and organics (McAdam et al., 2020b).

Additional future missions to Mars will also employ EGA-like analysis to search for organic molecules. The Mars Organic Molecule Analyzer (MOMA) onboard European Space Agency's ExoMars 2022 *Rosalind Franklin* rover will use pyrolysis gas chromatography-mass spectrometry (GCMS) and laser desorption spectroscopy to search for biosignatures on Mars. The *Rosalind Franklin* rover will land at Noachian (3.9 Ga) Oxia Planum, which appears to be a westward extension of the lower parts of the stratigraphy observed at Mawrth Vallis (Ivanov et al., 2020; Loizeau et al., 2020). Like Mawrth Vallis, strong and ubiquitous spectral signatures of dioctahedral Al-rich clay minerals overlying Fe/ Mg clay minerals suggests Oxia Planum may host remnants of a thick (~200 m) deep weathering profile or paleosol sequence that the rover could encounter during its primary mission.

1.4 Previous detections of organic carbon with SAM-EGA

Organic carbon has been detected in sedimentary rocks at Gale Crater with the SAM instrument using both QMS and GCMS (Ming et al., 2014; Rampe et al., 2014; Freissinet et al., 2015; Szopa et al., 2020). Abundances of reduced carbon were very low (< 1 wt. %) and restricted to three samples (Cumberland [CB], Confidence Hills [CH], and Mojave [MJ]). Though all CO_2 and CO detected to date is consistent with oxidized organic compounds, it is possible that contamination by the SAM-GCMS derivatization agent MTBSTFA could have resulted in these peaks. However, high-temperature (> 600° C) CO releases were consistent with indigenous oxidized martian organics. Additionally, chlorinated hydrocarbons (chlorobenzene [*m/z* 112], ~30 pmol) in the Cumberland drill sample and organo-sulfur compounds including thiophenes and thiols (~90 nmol) in the Mojave and Confidence Hills drill samples were identified in ~3.5 Ga mudstone, but the sources of these organic molecules was not constrained

(Freissinet et al., 2015; Eigenbrode et al., 2018). Observation of dichlorobenzene and trichloromethylpropane in the CB sample at Yellowknife Bay could have been produced by chemical reactions between organic molecules and oxychlorines occurring in the SAM ovens. These chlorinated hydrocarbons could have been derived from organic carbon, either from an indigenous martian source and/or from meteoritic infall (Fornaro et al., 2018; Szopa et al., 2020). Though organic carbon has been detected by SAM in numerous sedimentary rocks at Gale Crater, the source(s) of the organic molecules are not yet fully understood. Recent work has suggested that organic salts such as Ca/Mg oxalates and/or Ca/Mg acetates may be present in abundances of 1-2 wt. % in modern eolian sediments (Rocknest sample) as well as in ancient sedimentary rocks at Gale Crater (JK and CB samples) (Lewis et al., 2021). The accumulation of organic salts in eolian deposits suggests that they may be a component of regional or global dust on Mars (Lewis et al., 2021).

2. Methods

2.1 Sample collection

The paleosols examined in this study were collected from the Painted Hills Unit of the John Day Fossil Beds National Monument in eastern Oregon, USA. A previous study (Broz et al., 2022) determined the mineralogy and diagenetic alteration of the same set of samples examined in the present study. Samples from three individual paleosols in vertical succession were described and sampled approximately 7 km SW of the entrance to the Painted Hills unit (Lat: 44.631105, Long: -120.213107), in the Middle Big Basin Member of the John Day Formation, approximately 6 m above the local Eocene-Oligocene boundary (Figure 1, middle). Samples were chosen from this location because they were previously examined for mineralogy and diagenesis, and because $^{40}Ar/^{39}Ar$ dating of volcanic tuffs at this stratigraphic level in the section allow for a constrained age of 33.0 +/- 0.10 to 32.7 +/- 0.03 Ma (Biotite Tuff and Overlook Tuff, respectively) (Bestland, 1997).

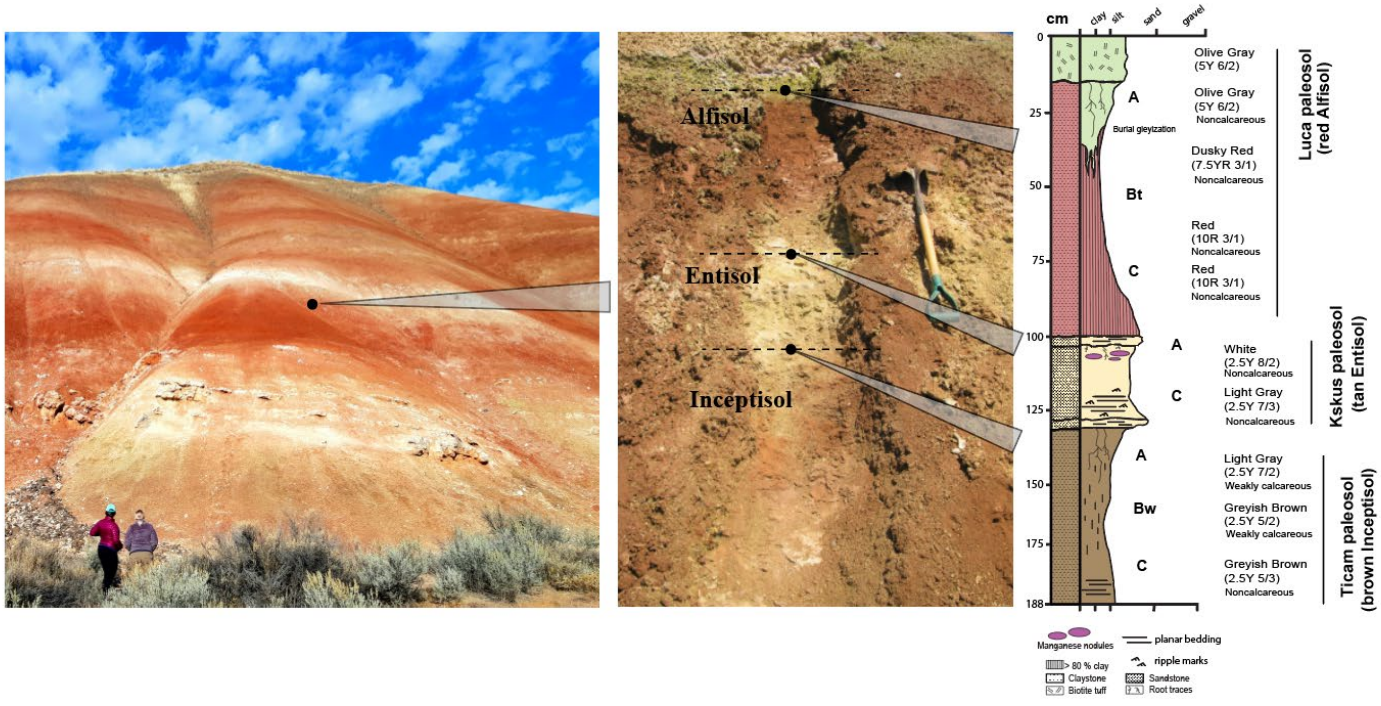

Figure 2. Morphology of three successive paleosols from the early Oligocene (33 Ma) middle Big Basin Member of the John Day Formation in eastern Oregon, USA showing lithology, grain size, horizon designations, and Munsell color. The upper paleosol (red with drab green top) is a moderately weathered red Alfisol (Hapludalf in USDA Taxonomy); stratigraphically below is a minimally weathered and weakly developed Entisol (Fluvent; tan color); the lowest soil (brown color) is an Inceptisol (Andic Eutrochrept, brown color).

To minimize contamination from modern organic carbon during sampling, all loose surface soil and saprolite was removed until the lithified, brick-like unweathered paleosol surface was exposed. Below the saprolite of the thin (~30 cm) modern soil, all three paleosols were lithified claystone. Before collection, all sampling and storage materials were ashed at 550° C to remove organic contaminants. Sample collection for evolved gas analysis (EGA) began by trenching with a rock hammer to a ~30 cm depth into (perpendicular to) the lithified paleosol sequence. Next, a set of samples were gathered down a vertical transect at approximately 10 cm intervals, similar to sampling the horizons of a modern soil. Large (~1 kg) lithified blocks of claystone were broken out of the outcrop and placed into aluminum foil to ensure subsampling for thermal analysis had sufficient volume to expose fresh sample surface (e.g., no weathered surfaces were selected for analysis). Small (5-8 g) subsamples were acquired from the inside of bulk lithified samples with steel chisels. These subsamples were then ground to < 0.02 mm using an agate mortar and pestle and stored in glass vials prior to thermal analysis and radiocarbon dating. No vegetation was present within ~30 m of the sampled paleosol sequence (Figure 2), likely because the “popcorn” weathering of the smectite-rich modern soil appears to inhibit plant germination and growth. The Munsell

color and qualitative calcareousness of samples were described during collection. The three paleosols sampled were a red Alfisol ("Luca" pedotype from (Retallack et al., 2000), a tan Entisol ("Kskus" pedotype), and a brown Inceptisol ("Ticam" pedotype, Figure 2).

2.2 Radiocarbon dating of organic carbon in paleosols

The purpose of radiocarbon (^{14}C) dating was to constrain the age of organic carbon in paleosol samples. Specifically, radiocarbon dating was used to determine if the organic carbon fraction of paleosols was entirely endogenous (e.g., autochthonous, deposited during soil formation) and had been preserved for millions of years, or if there had been additions of exogenous (allochthonous) organic carbon to paleosols in the last ~45,000 years (a typical method-level detection limit for radiocarbon dating techniques).

For radiocarbon analysis, samples were gathered by trenching at a horizontal angle into the outcrop, whereas sampling for EGA was performed vertically (down section) once the surface soil had been removed from the outcrop (Figure 2). In other words, EGA samples were collected down section (e.g., vertical depth in the section) whereas radiocarbon samples were obtained by trenching further into the outcrop (e.g., horizontal depth into the outcrop) at the vertical intervals where EGA samples were collected. The purpose of this sampling difference was to help determine if the horizontal sampling depth into the outcrop was related to the amount of radiocarbon accumulation in the brick-like paleosol samples collected within ~0.5 meters of the modern weathering zone.

A radiocarbon age of organic carbon was obtained from four samples, two from the exposed surface and near-surface horizons (A and Bt horizons) of the stratigraphically highest soil (Alfisol) and two from the surface and near-surface horizons of the stratigraphically lowest profile (Inceptisol). All samples for radiocarbon dating were acid-washed to remove inorganic carbonates. Ground paleosol samples (~5 g) were treated with approximately 20 mL of 0.1 M HCl at room temperature for 1 hour, then washed three times with ~30 ml of deionized water and dried at 60° C for 24 hr. Radiocarbon dating of acid-washed paleosol samples was performed at the W.M. Keck Carbon Cycle Accelerator Mass Spectrometer at the University of California, Irvine. Additional TOC determination of these samples was performed at UC Irvine and are reported in Table 1. The accuracy and precision (1 σ) of this analysis on modern carbon ($\Delta^{14}C$ >0‰) was better than 9‰. Laboratory blanks yielded a $\Delta^{14}C$ value of -996.2 ‰.

Quantifying additions of modern carbon to bulk paleosol samples

Calibrated radiocarbon dates, taken at face value, may represent a mixture of radiocarbon-free Oligocene carbon and some amount of post-bomb modern organic carbon. To test the hypothesis that

paleosols contained modern organic carbon, we used a two-endmember mixing model to estimate the relative proportion of modern carbon in bulk paleosol samples. Based on the distinct isotopic composition of modern organic carbon and radiocarbon-free Oligocene carbon, a two-endmember mixing model (Sickman et al., 2010; Silva et al., 2013) was used to quantify the relative proportions of modern and ancient carbon as distinct sources of the paleosol organic carbon pool (Zech et al., 2017). We used the following equation to partition modern organic carbon sources ($D^{14}C$ = 0 ‰) from radiocarbon-dead Oligocene organic carbon ($D^{14}C$ ~ -999‰):

$$\mathbf{C_{modern} = C_t(D^{14}C_{bulk} - D^{14}C_{Oligocene})/(D^{14}C_{Modern} - D^{14}C_{Oligocene})} \quad \mathbf{(1)}$$

Where C_t is the total amount of organic carbon (TOC) measured in bulk samples, $D^{14}C_{bulk}$ is the measured $D^{14}C$ value of bulk samples, $D^{14}C_{Modern}$ is a typical value for a modern organic carbon endmember ($D^{14}C$ = 0 ‰), $D^{14}C_{Oligocene}$ is a typical $D^{14}C$ value for a radiocarbon-free organic carbon endmember ($D^{14}C$ = -999‰), and C_{modern} is the modelled fraction of modern organic carbon in bulk samples. Errors were propagated to estimate uncertainty associated with modelled values. The sources of uncertainty considered in the model were a) the uncertainty of the measured TOC values and b) uncertainty of the measured $D^{14}C$ values, both from analysis of duplicate samples.

2.3 Thermal and evolved gas analysis of paleosol samples

The purpose of this work was to use SAM-EGA-like conditions to characterize bulk gas evolution and to measure abundance of organic and inorganic carbon in Mars-analog paleosol samples. A Setaram Labsys Evo differential scanning calorimeter (DSC) / thermal gravimeter (TG) connected to a Pfeiffer Omnistar QMS was configured to operate similarly to the SAM evolved gas analyzer. The SAM instrument does not have TG/DSC capabilities, but these components permit a better understanding of phase transitions and chemical reactions in laboratory experiments. Approximately 50 mg ± 3 mg of ground paleosol sample (previously stored in glass vials ashed at 550° C to minimize organic contamination) were placed in an Al_2O_3 sample crucible (also previously ashed at 550° C). The sample crucible and an identical empty reference crucible were placed in the furnace and then the system was purged twice with helium gas and set to a pressure of 3 kPa. Helium was chosen as a carrier gas because it is inert and because it used as a carrier gas in the SAM instrument. The crucibles were heated from approximately 35 °C to 1000 °C at a heating rate of 35°C/min and at a flow rate of 10 cm^3/s. Volatiles ranging from mass/charge (*m/z*) 1 - 100 were measured. All analyses were performed in duplicate.

Total organic carbon (TOC) content was determined using a Netzsch TG/DSC coupled to a Pfeiffer QMS using a modified method of Fernández et al., (2012). An Al_2O_3 sample crucible and an identical reference crucible were placed in the furnace. The instrument was purged twice with ultra-high purity O_2 and set to a pressure of 1000 mbar prior to sample analyses to remove any contamination in the system. Oxygen was chosen as a carrier gas because it encourages complete combustion of all organic and inorganic carbon in samples. The crucibles containing samples were heated from approximately 35 °C to 1000 °C at a heating rate of 35°C/min and at a flow rate of 19 ml O_2/min. A series of three blanks were analyzed before and after each group (n=10) of samples. A calibration curve for CO_2 was created by analyzing a calcite standard (Iceland sparry calcite 40μM) at eight sample masses ranging from 0.01 – 4 mg (Table S1). This calibration curve was used to calculate the amount of CO_2 evolved from each sample, and these values were used to calculate total carbon in each sample (Table S2). Errors ranged from 0.01 – 0.003 wt. % carbon.

Thermal techniques including TG-DSC-EGA allow for quantitative estimates of organic and inorganic carbon without sample pretreatment, in part due to the large differences in thermodynamics and peak CO_2 release temperatures. By contrast, TOC determinations via elemental analysis involve an acid pretreatment step to remove carbonates. Paleosol samples were not acid-pretreated for thermal and evolved gas analyses because some organic carbon can be oxidized during acid-washing (e.g., Apesteguia et al., 2018). In the present study, carbon was considered organic between 150-550° C and inorganic from ~700-900° C. Total organic carbon was quantified by deconvolving CO_2 peaks if a carbonate-C peak was present. This was done by determining the relative percentage of peak area from inorganic carbon-evolved CO_2 (~700-900° C) then subtracting this value from total carbon-evolved CO_2 peak area to solve for TOC. All evolved gas plots were background-corrected to account for possible atmospheric contamination.

3. Results/Discussion

3.1 Radiocarbon dating of paleosol organic carbon

Radiocarbon dating of four samples from two different paleosol profiles showed raw $D^{14}C$ values ranging from -539.1‰ ± 1.3‰ to -836.7‰ ± 3.4‰ and calibrated ages between 6,265 ± 25 years BP and 14,560 ± 170 years BP (Table 1). The fraction of modern carbon (FM) ranged from 0.469 ± 0.039 to 0.1633 ± 0.034 (Table 1) and was highest in the surface horizon of the Alfisol and lowest in the subsurface horizon, suggesting this paleosol contained a mixture of ancient and modern organic carbon. These samples all showed a distinct signature of exogenous organic carbon because the samples were not radiocarbon dead (^{14}C-free). Two hypotheses to explain the radiocarbon dates are A) additions of modern

organic carbon to bulk samples (e.g., a $D^{14}C$ ~ 0‰ modern carbon pool mixing with an ancient, radiocarbon-free pool) or B) a Holocene (6-14 Ka) productivity event introduced carbon into the paleosols (e.g., the carbon is indeed tens of thousands of years old).

One possible source of exogenous organic carbon may derive from precipitation-driven leaching of dissolved organic carbon from modern biota living in the current weathering zone above the paleosol outcrop. As such, it is possible that small amounts of exogenous modern organic carbon from the weathered zone above paleosol outcrops have mixed with larger amounts of ^{14}C-free organic carbon endogenous to paleosols. In this way, a radiocarbon date of ~6-14 Ka BP could represent a mixing of modern organic carbon and ~33 Ma organic carbon. This hypothesis is supported by the erosion rate for the site, which was previously determined to be approximately 4.94 ± 0.05 mm/yr. (Sweeney et al., 2015). Using this erosion rate, the 20 cm-thick soils that formed on top of the paleosol outcrops are only about 40 years old and could have leached modern organics into the underlying paleosols during this time.

Table 1. Radiocarbon dates and application of a two-endmember isotopic mixing model to measured $D^{14}C$ values from four bulk paleosol samples. Depth (cm) represents the horizontal depth into the outcrop from where samples were gathered. TOC, total organic carbon; FM, fraction of modern.

Sample ID	Depth (cm)	TOC (%)	TOC ±	FM	$D^{14}C$	±	^{14}C age (years BP)	±	Modern carbon (%)	±
Alfisol	32	0.015	0.001	0.163	-836.7	3.4	**14560**	170	0.487	0.066
Alfisol	14	0.010	0.001	0.461	-539.1	3.9	**6220**	70	3.141	0.105
Inceptisol	20	0.031	0.001	0.459	-541.5	1.3	**6265**	25	0.916	0.032
Inceptisol	22	0.018	0.001	0.437	-563.3	1.8	**6655**	35	0.872	0.056

Application of a two-endmember isotopic mixing model to raw $D^{14}C$ values (Equation 1) for estimation of modern organic carbon abundances in bulk paleosol samples is shown in Table 1. The modelled abundances of modern carbon ranged from 0.487 ± 0.066 % and 3.141 ± 0.105 % of the total organic carbon in each sample. These results support the hypothesis that the measured $D^{14}C$ values represent the mixing of small amounts of modern organic carbon with larger amounts of presumably radiocarbon-free Oligocene carbon. There was also a significant power law relationship between the modeled organic carbon abundance and the horizontal depth into the profile from where the sample was collected (**$y = 21.518x^{-0.418}$, $R^2 = 0.9194$**, **Figure S1).** Modelled abundances of modern carbon in samples from shallower horizontal depths in the outcrop were significantly ($P < 0.053$) greater compared to samples from deeper depths (Figure S1), which was consistent with precipitation-driven leaching of modern organic carbon into paleosol outcrops. Due to the limited sample size (n=4), additional efforts are needed to determine if this relationship exists across larger samples sizes and within deeper transects

(e.g., > 100 cm). In summary, additions of exogenous carbon were most likely modern (last 40 years), rather than from the Holocene (6-14 Ka). However, results from this work alone cannot definitively exclude the possibility of a Holocene productivity event which could have led to leaching of carbon into ancient samples during that time. These results demonstrate that a radiocarbon approach can be a useful technique for constraining the age and sources of organic carbon in ancient pedogenic samples.

3.2 Thermal and Evolved Gas Analysis

3.2.1 CO_2 and CO evolutions

When subject to thermal and evolved gas analysis, all samples evolved CO_2 at temperatures ranging from ~150 – 800° C and had two to three distinctive CO_2 peaks (Figure 3). In several of the samples, a broad low temperature ~200 - 500° C peak was followed by a well-resolved (e.g., sharp) high-temperature peak at ~650-750° C. Four of the six samples also showed a well-resolved CO_2 peak at 600° C which was consistent with the decomposition of inorganic carbon. In general, CO_2 evolved at 150-500° C is primarily from organic carbon decomposition (Sutter et al., 2017; Apesteguia et al., 2018) but also possible are contributions are from CO_2 inclusions in minerals or amorphous phases. The organic C contributing to evolved CO_2 is most likely from simple organic compounds (~350° C) or refractory macromolecular organic compounds (300-600° C) (Eigenbrode et al., 2018). Table 2 shows the calculated organic carbon content of EGA samples.

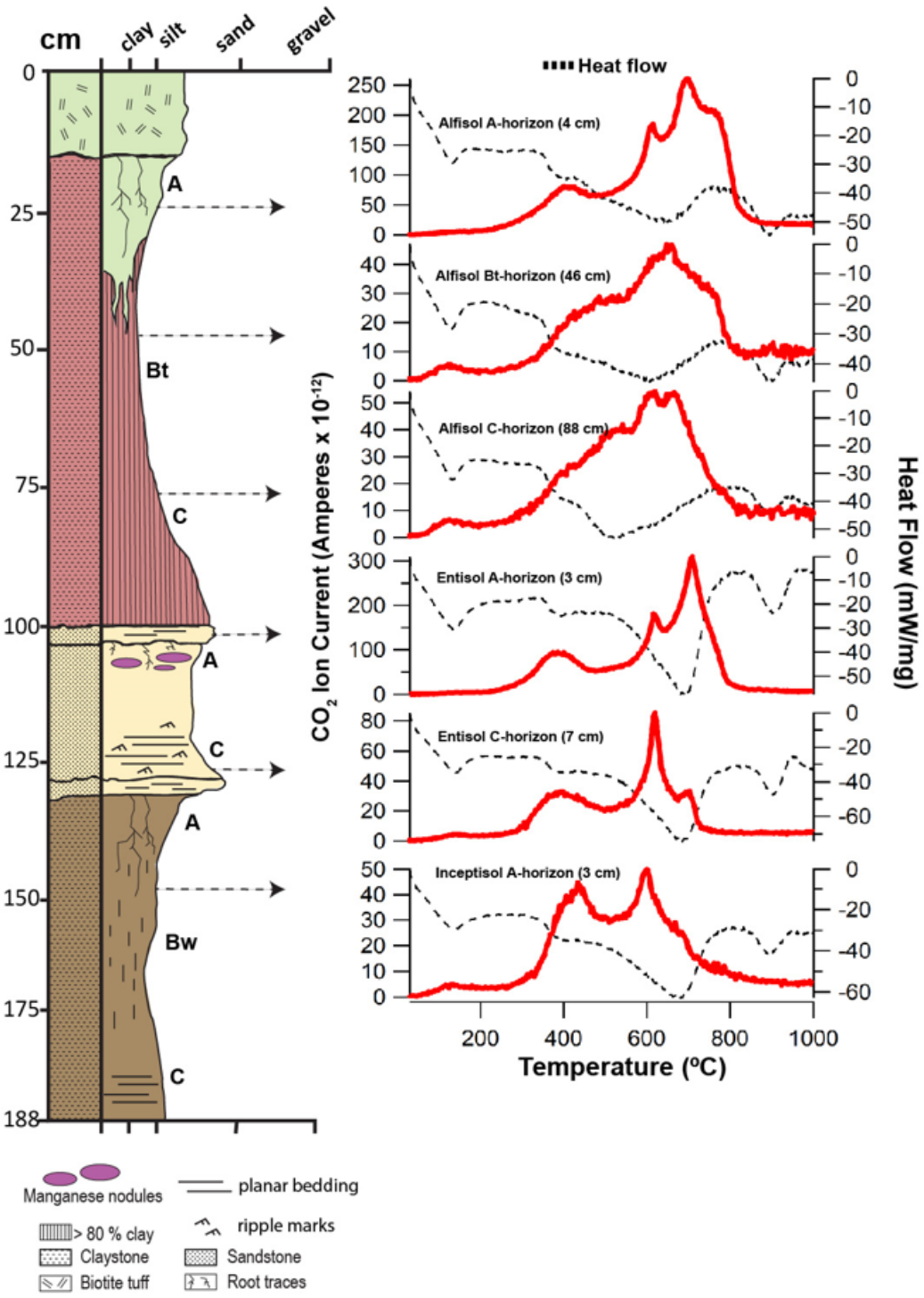

Figure 3. Evolutions of CO_2 (red traces) and heat flow (dashed traces) from early Oligocene (33 Ma) Al/Fe smectite-rich paleosols from the John Day Fossil Beds National Monument, Oregon. Red trace is CO_2 (*m/z* 44) and dashed trace is heat flow from differential scanning calorimetry (DSC). Helium was used as a carrier gas for all analyses.

Table 2. Total organic carbon (TOC) and total inorganic carbon (TIC) of paleosols examined in this study. Depth (cm) represents the vertical depth of each paleosol profile within the measured stratigraphic section

Paleosol	Horizon [φ]	Depth (cm)	Total C (wt. %)	TOC (wt. %)[†]	±σ TOC [§]	TIC (wt. %)
Alfisol	A	4	0.073	0.031	0.0062	0.042
Alfisol	A	14	0.094	0.026	0.0097	0.068
Alfisol	Bt_1	46	0.021	0.018	0.0016	0.003
Alfisol	Bt_2	63	0.067	ND [ʊ]	-	0.067
Alfisol	C	88	0.033	0.002	0.007	0.031
Entisol	A	100	0.046	0.021	0.0068	0.024
Entisol	C	120	0.036	0.013	0.0037	0.024
Inceptisol	A	125	0.024	0.018	0.007	0.006
Inceptisol	Bw_1	131	0.027	0.008	0.0013	0.019
Inceptisol	Bw_2	160	0.020	0.011	0.0023	0.010
Inceptisol	C	175	0.026	0.001	0.0013	0.026

[φ] Horizons follow USDA Soil Survey Staff (2014) major horizon designations
† Determined by thermal analysis (TG-DSC-EGA) without acid pre-treatment of samples; average of two duplicates.
ʊ ND = No detection; below limit of quantification
[§] Standard error for TOC determination from duplicate analysis

The endothermic thermal decomposition of Ca carbonate was a probable source of CO_2 release from approximately 550 – 800° C (Figure 3) (Cannon et al., 2012; Sutter et al., 2012). High temperature (> 650° C) CO_2 evolutions generally exceeded the low temperature (150-550° C) CO_2 evolutions in peak area across all samples. Total inorganic carbon (TIC) values varied from 0.006 to 0.068 wt. % (Table 2) and the ratio of inorganic carbon to total carbon ranged from 0.14 to 1, consistent with variable mixtures of Ca carbonate and organic carbon in each sample. There are well-defined Ca carbonate endotherms in the heat flow data from the Entisol and Inceptisol, but this trend was not so well-defined in the Alfisol (Figure 3) and there also appears to be "doublet" high-temperature CO_2 peaks for the Entisol, suggesting a combination of Ca-carbonate and perhaps dolomite or ankerite, though these phases were not previously observed with XRD (Table S3 and Figure S2). DSC-EGA analysis of modern soils containing various amounts of calcite have a similar sharp endothermic CO_2 peak release temperature at ~700° C that was attributed to the thermal decomposition of Ca carbonate (Apesteguia et al., 2018). An additional ~900° C endotherm observed in all samples was unrelated to carbonate decomposition and instead was attributed to thermal decomposition of sulfate minerals such as jarosite, which was previously detected in trace amounts with x-ray diffraction (Tables S3 and S4). Interestingly, Ca-carbonate was not previously identified from x-ray diffraction patterns (Table S3 and Figure S2), and thus it is likely that these samples contain inorganic carbon below detection limit of XRD (~1 wt. %), but not SAM-EGA (0.01 wt. %). This agrees with estimated abundances of TIC, which were below 1 wt. % (Table 1) and demonstrates the

ability of SAM-EGA-like analyses to detect trace amounts of inorganic carbon in complex pedogenic mineral matrices.

Other sources of high temperature CO_2 release could have result from the decarboxylation of organic compounds in refractory or thermally mature organic matter that occur over a broad range of temperatures (150 - 800° C). Previous investigation showed no coalification of organic matter or development of secondary porosity in any paleosols from the Painted Hills, which were buried by an estimated 1.5 - 2 km of overburden (Retallack et al., 2000; Horgan, 2016), suggesting paleosol samples here contain refractory but not thermally mature organic compounds.

All samples evolved CO with a peak release temperature of ~350° C (Figure 4). Evolution of CO was consistent with incomplete combustion of organics and/ or the presence of oxygen-bearing organics (Sutter et al., 2017). We did not observe clear co-evolutions of CO and CO_2 because the peak release temperature for CO was ~50° C lower than for CO_2 (Figure 4), but there was a distinct overlap in the peak release temperature (e.g., they have overlapping elution times, but they are not coeluting) suggesting that a portion of the CO could have been released from incomplete combustion of organic carbon. The co-occurrence of CO and CO_2 was not observed at high (~700 °C) temperatures (Figure 4) because the thermal decomposition of Ca carbonate does not produce CO. Thus, evolved CO detections near 400° C were consistent with the decomposition of organic compounds.

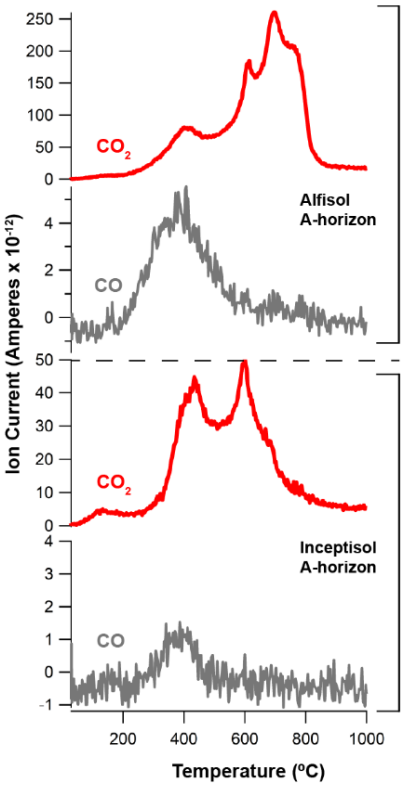

493 **Figure 4. CO_2 (red trace) and CO (*m/z* 28) (grey trace) evolutions from the surface horizons of paleosols at the**
494 **John Day Fossil Beds National Monument, Oregon.** Top panel is surface (4 cm) horizon of an Alfisol; bottom
495 panel is surface (3 cm) horizon of an Inceptisol.
496

497 ### 3.2.2 NO evolutions

498 Nitric oxide (NO; *m/z* 30) was detected in all paleosol samples (Figure 5) and was consistent with
499 the oxidation of nitrogen-bearing organics. In the sample with the greatest amount of organic carbon
500 (Alfisol A-horizon), evolutions of NO start at ~300° C and show peak release temperature of ~ 400° C as
501 well as a small shoulder at ~ 600° C (Figure 5). Additionally, organic fragments observed in this sample
502 included CH_2 (*m/z* 14), CH_3 (*m/z* 15), and C_2H_2 (*m/z* 26) (Figure 6). Evolutions of NO were simultaneous
503 with evolutions of these organic fragments at ~400° C, suggesting the oxidation of a nitrogen-bearing
504 organic compound was a significant contributor to evolved NO (Navarro-González et al., 2009).
505

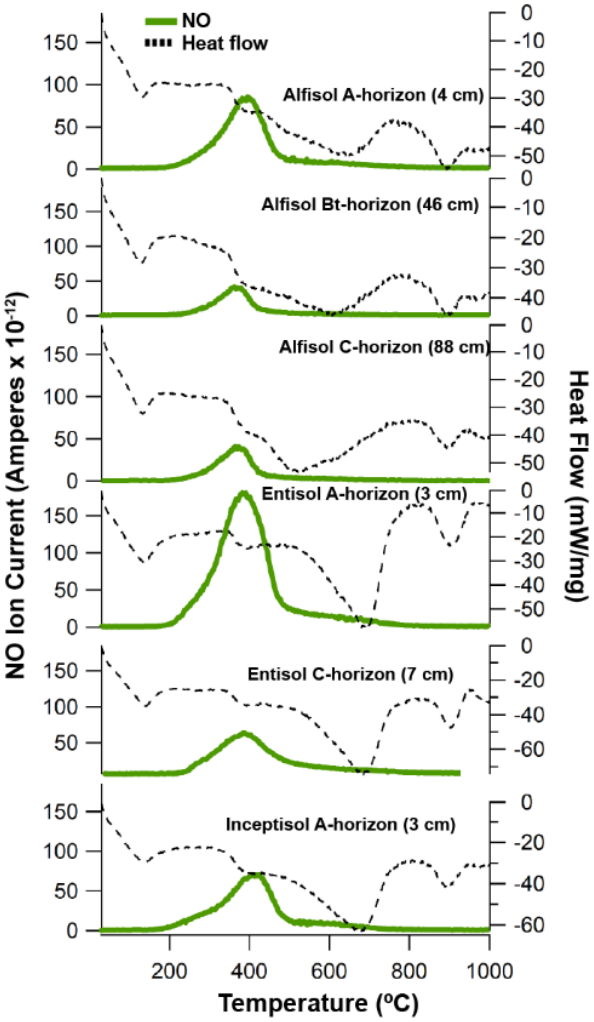

506
507 **Figure 5. Evolutions of nitric oxide (NO) from paleosols at the John Day Fossil Beds National Monument,**
508 **Oregon.** Green trace is NO (*m/z* 30) and dashed trace is heat flow from differential scanning calorimetry (DSC).

The thermal decomposition of nitrates can also release NO, though at elevated temperatures (> 500° C) relative to nitrogenated organics (Stern et al., 2015), and therefore the NO release temperate can constrain the origin of NO. For example Alkali (Na, K) and alkaline earth (Mg, Ca) metal nitrates decompose to NO at temperatures > 560° C (Stern et al., 2015). In laboratory experiments under SAM-like conditions, $Fe(NO_3)_3$ begins to decompose to NO at < 200° C and exhibits two distinct releases of NO at ~300 and ~450° C, which has been attributed to dehydration and hydrolysis of $Fe(NO_3)_3$ hydrates, respectively (Stern et al., 2015). Instead, NO release in paleosol samples begins at ~250° C and exhibited a single peak at ~400° C across all samples (Figure 5), unlike the dual high-temperature NO peaks from decomposition of $Fe(NO_3)_3$ hydrates. The simultaneous evolution of NO, CO_2, and organic fragments in paleosol samples analyzed here (Figure 6) are an additional line of evidence suggesting NO releases could have resulted from oxidation and/or decarboxylation of nitrogen-bearing organic compounds. We also observed evolutions of small nitrogen-bearing organics (HCN, m/z 27, 26) that co-occurred with evolutions of NO (m/z 30) in several samples, including the surface horizon of the Alfisol (Figure S5).

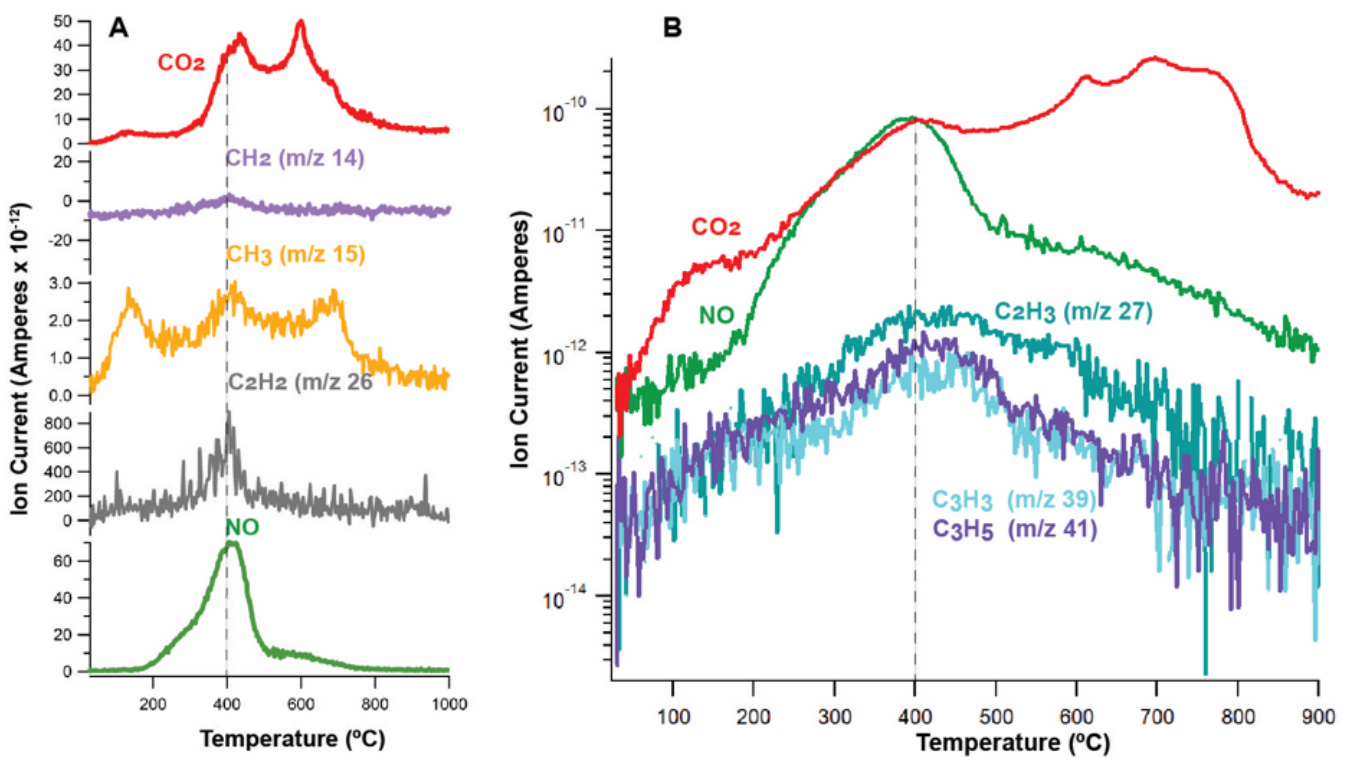

Figure 6. Simultaneous evolutions of CO_2, NO (*m/z* 30) and organic fragments in paleosol surface horizons. **(A)** Evolutions of CO_2, NO (*m/z* 30), and organic fragments (*m/z* 14, 15, 26) from the surface horizon of the Inceptisol (3 cm). **(B)** Semi-log scale plot of CO_2, NO and additional organic fragments (*m/z* 27, 39, 41) from the surface horizon (4 cm) of the Alfisol

One possible source of nitrogen-bearing organic carbon compounds is pyrogenic carbon (char) in paleosol samples that formed as a result of wildfires across the original soil landscape (Kurth et al., 2006). Nitrogen-bearing organic compounds such as nitriles, pyridine and pyrrole-derive compounds have been observed with pyrolysis GC/MS in modern fire-affected soils (De la Rosa et al., 2008). These modern soils were also observed to have a broad ~400° C peak release temperature of NO (*m/z* 30) during TG-DSC-EGA, suggesting that pyrogenic carbon may be the source of low-temperature NO release in soils. However, the fire history of paleosols in the present study has not yet been investigated. Although it is impossible to determine the original inputs of nitrogen-bearing organics in paleosols, nitrogen may have been incorporated into increasingly stable organic matter as a consequence of forest fires, and may persist in paleosols today as char. Previous authors have reported the occurrence of preserved char in paleosols of late Permian (Miller et al., 1996) and late Jurassic age (Matthewman et al., 2012), so it is plausible that nitrogen-bearing char may be responsible for the overlapping ~400° C NO and CO_2 peaks observed here.

3.3 Possible mechanisms of organic carbon preservation in paleosols

There are many competing factors that control the preservation and degradation of organic carbon in terrestrial environments. Minerals themselves may facilitate oxidation of organic carbon compounds (Kleber et al., 2021), as is the case with certain Mn-bearing minerals (Reardon et al., 2016). Paleosols examined here contained between ~70-90 wt. % smectite, primarily as mixtures of montmorillonite and nontronite (Tables S3 and S5). Possible mechanisms of organic carbon preservation include the formation of organo-mineral complexes, and/or the formation of microaggregates that may have increased the biochemical stability of organic molecules, as observed in modern soils (Plante et al., 2011) and Quaternary paleosols (Marin-Spiotta et al., 2014). Smectite clay minerals in particular preserve organic molecules due to their high specific surface area, negatively charged interlayers, and cations that inhibit water flow, thus making them favorable locations for the preservation of organic carbon over millions or possibly billions of years (Bishop et al., 2013; Noe Dobrea et al., 2016; Szopa et al., 2020).

We observed evolutions of volatile gases from clay-rich paleosols that may have resulted from the preservation of organic carbon over geological time scales, as well as possible contributions from small amounts of modern organic carbon detected with radiocarbon analysis. The fragmentation of organic molecules during pyrolysis EGA provides limited constraints on the types of molecules present, but it can help determine if there are any associations between minerals and organic molecules. These associations can include physical occlusion, chemisorption and/or adsorption to mineral surfaces, or intercalation in clay minerals (Kleber et al., 2005, 2021; Schmidt et al., 2011; François et al., 2015). A strong correlation between the peak release temperature of organic fragments and the release of H_2O or other volatiles would suggest that organic matter could have been associated with minerals.

564 In all samples, there were no apparent co-occurring evolutions of organic fragments, CO_2, and
565 water releases from clay dehydroxylation (Figure 7). The Al-smectite in the surface horizon of the Alfisol
566 began dehydroxylation near 400° C. Figure 7 shows the peak release temperature of organics and CO_2
567 was ~100° C lower relative to peak H_2O release from Al-smectite dehydroxylation. This sample had the
568 highest TOC (~0.03 wt. %), FM of ~0.46 (Table 1), and a phyllosilicate content of ~85 wt. **%** (Table S3).
569 Interestingly, samples from other depths had higher temperatures of clay dehydroxylation due to
570 differences in clay mineralogy and/or abundance, such as the Entisol and Alfisol (Figures S3 and S4), but
571 these samples were depleted in organic carbon relative to the Al smectite-rich surface horizon of the
572 Alfisol (Table 1). Though our EGA results do not provide evidence that phyllosilicates and organics were
573 strongly associated with one another, it is possible that the high clay mineral abundances provided other
574 means of organic preservation, including physical occlusion, the formation of organic-mineral aggregates,
575 or other weaker types of sorption to phyllosilicate surfaces, such as outer-sphere complexation
576 (Guggenberger and Kaiser, 2003; Schmidt et al., 2011).
577

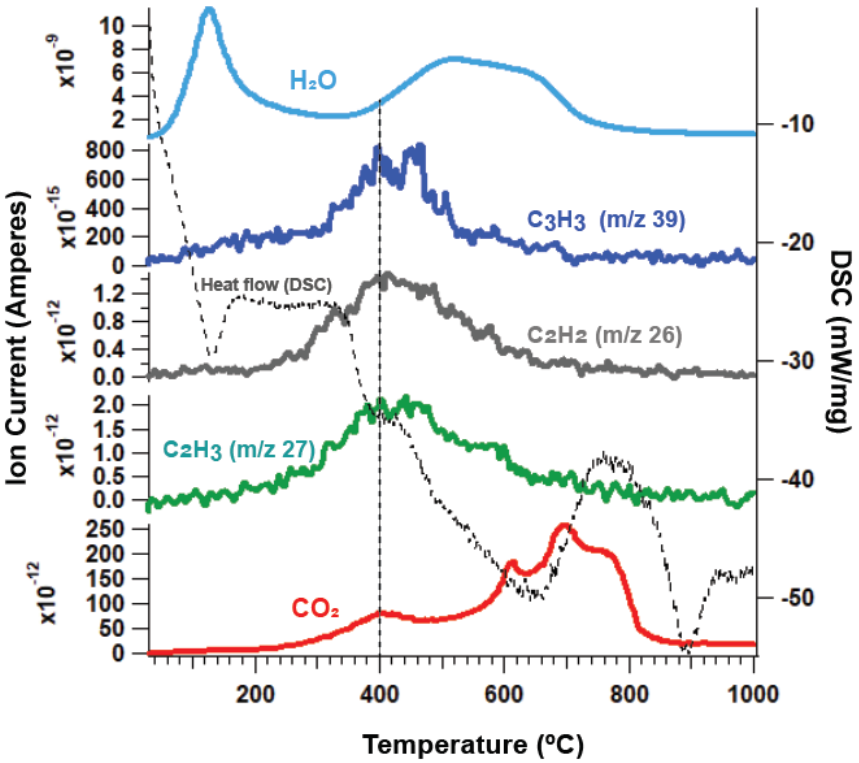

578
579 **Figure 7. Evolutions of CO_2, organic fragments, and H_2O from the surface horizon of the Alfisol (4 cm).** Co-
580 occurring releases of CO_2 and organic fragments at the onset of Al-smectite dehydroxylation (H_2O release at ~400°
581 C, vertical dotted line) suggest organic molecules may have been associated with clay minerals. Dashed trace is heat
582 flow from differential scanning calorimetry (DSC).
583

584 Interactions with sulfur can also aid in the preservation of organic molecules in soils and
585 sediments over geological time scales (Matthewman et al., 2012; François et al., 2015; Eigenbrode et al.,
586 2018; Alekseeva et al., 2019). The incorporation of organic C into the crystal lattice of sulfate minerals
587 can increase thermodynamic stability and therefore increase the temperature of organic carbon
588 decomposition during EGA (François et al., 2015). Minor detections of jarosite and gypsum in XRD
589 patterns (< 5 wt. %) were observed, and these minerals could have also contributed to the preservation of
590 organics (Tables S5 and S6). Minor SO_2 evolutions at ~800° C across all samples (Figure S3) were
591 consistent with the decomposition of sulfate minerals. A single sample (Entisol 7 cm) had a low-
592 temperature SO_2 peak that co-occurred with the CO_2 release at ~400° C (Figure 8).

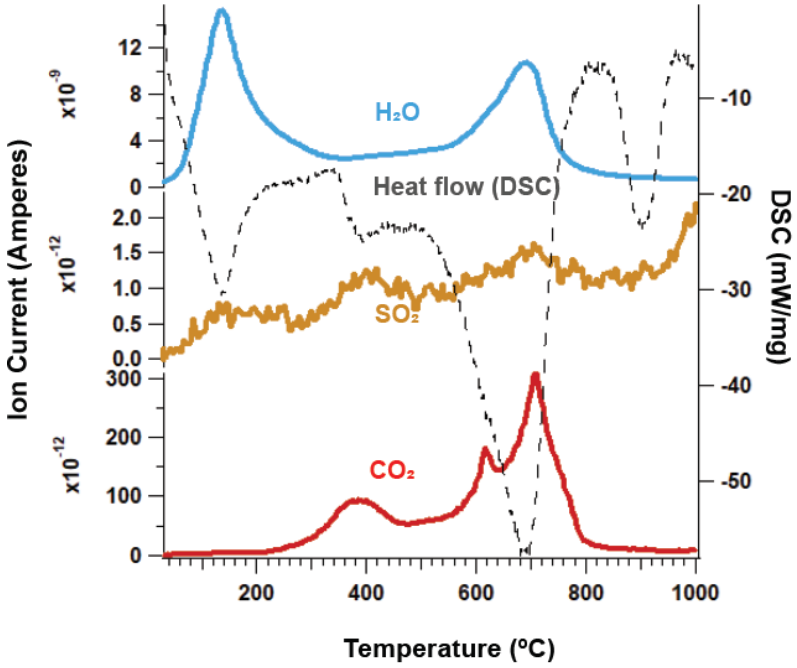

593
594 **Figure 8. Evolutions of H_2O (blue trace), SO_2 (yellow trace), CO_2 (red trace), and heat flow (dashed trace)**
595 **from the surface horizon of the Entisol (3 cm).** DSC – differential scanning calorimetry (heat flow), H_2O – *m/z*
596 18, SO_2 – *m/z* 64, CO_2 – *m/z* 44.
597
598 Trace amounts of Mg sulfates in the Alfisol could account for minor SO_2 releases > 700° C
599 including the ~790° C SO_2 peaks (François et al., 2015; Mcdam et al., 2020a). At higher temperatures, all
600 soils showed a major release of SO_2 beginning at 900° C that co-occurred with an endotherm, both of
601 which are consistent with the thermal decomposition of crystalline sulfates (Ming et al., 2014; François et
602 al., 2015). Since the samples were only heated to ~1000° C for this work, the maximum peak height of
603 this release cannot be ascertained. Peak SO_2 release temperatures generally did not co-occur with low-
604 temperature (~400° C) CO_2 evolutions across the rest of the samples (Figure S3), so it is unlikely that
605 sulfate minerals played a significant role in organic preservation in samples examined here. However, it

606 has been hypothesized that sulfate minerals were most likely diagenetic and not original to the paleosols,
607 but instead were inherited from the modern weathering zone (Broz et al., 2022). Thus, if modern sulfate
608 minerals were associated with small amounts of modern organic carbon, the sulfate minerals could have
609 been a source of radiocarbon in samples with co-occurring SO_2 and CO_2 evolutions.
610
611
612 **3.4 Enrichment of organic carbon in surface layers of paleosols**
613 The near-surface horizons of all paleosols examined here had greater amounts of total organic
614 carbon (TOC) relative to deeper horizons (Figure 9, Table 1). The highest amounts of CO_2 released from
615 decomposition of organic carbon (150-500° C) were in the near surface (A) horizons of all three paleosol
616 types while subsurface layers of paleosols generally had lower quantities of evolved CO_2 from organic
617 carbon (Figure 3, Table 1). The A horizon of the Alfisol had TOC of 0.031 ± 0.006 wt. % and
618 progressively decreased to 0.002 ± 0.007 wt. % in the C horizon.

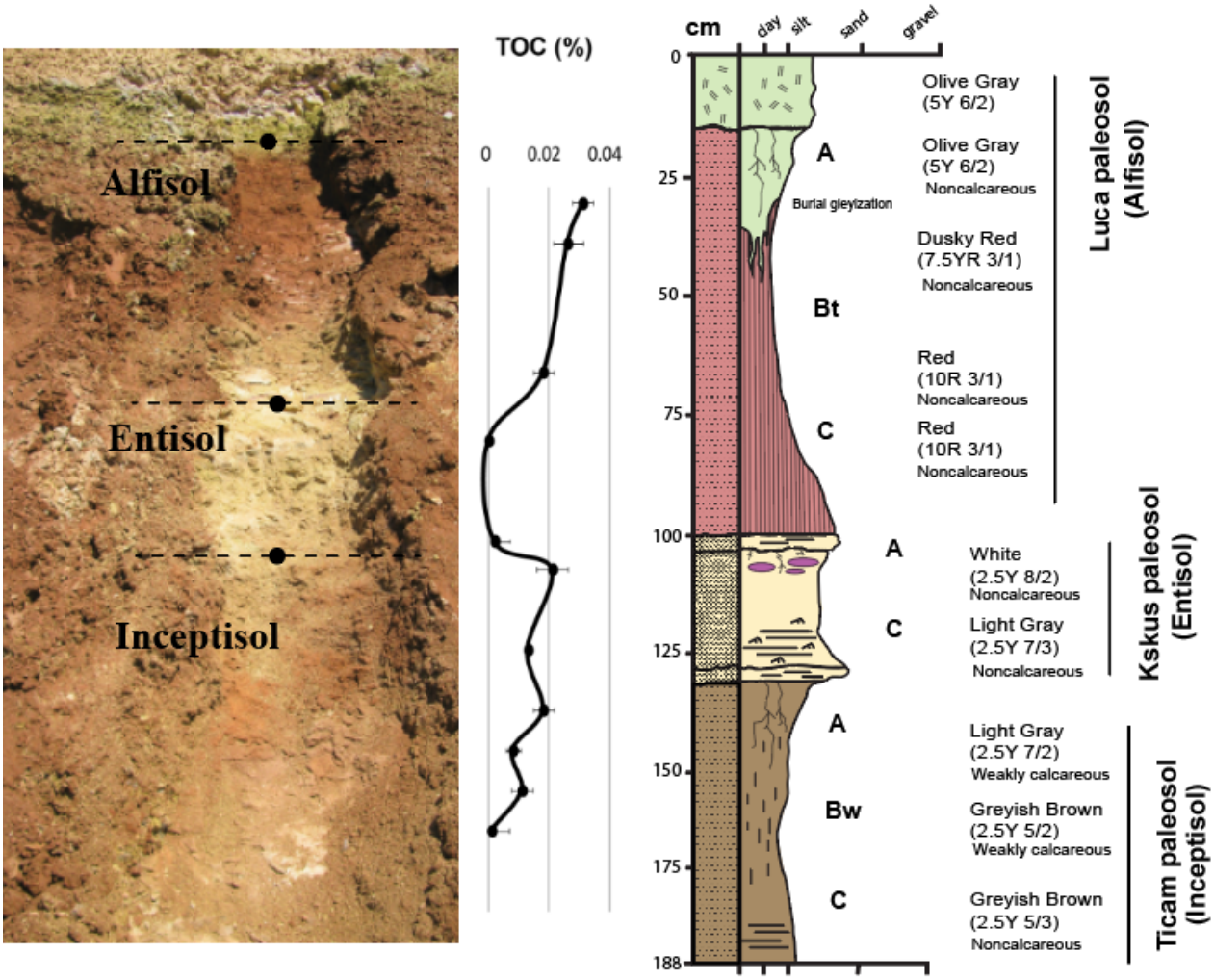

619

620 **Figure 9. Trends of organic carbon enrichment in the near-surface horizons of three paleosols** from the early
621 Oligocene (33 Ma) middle Big Basin Member of the John Day Formation in eastern Oregon, USA**.** The surface (A)
622 horizons of all three profiles had significantly ($P > 0.05$) higher total organic carbon (TOC) content relative to
623 subsurface horizons (Bt, Bw and C horizons, respectively). Average TOC content of samples (n=2) was determined
624 by thermal and evolved gas analysis (oxygen as a carrier gas).
625

626 Samples from the A-horizon of the Alfisol had been affected by burial gleization (Broz et al.,
627 2022). Burial gleization is an early diagenetic process in paleosols that involves the reduction of Fe^{3+} to
628 Fe^{2+} by anaerobic microbes as a result of rapid burial (PiPujol and Buurman, 1994; Retallack, 2019). This
629 is also thought to promote anaerobic decay of organic matter (Retallack, 2019), even in soils that
630 originally formed under oxidizing conditions before burial. Typical burial gleization is closed system
631 alteration, without depletion of total iron, and is usually limited to the surface horizons where organic
632 matter is most concentrated. The surface horizon of the Alfisol examined in this work showed classic
633 evidence of burial gleization with drab-colored mottles and tubular features predominantly in the A-
634 horizon with minor radiation downward into the subsurface (Bt) horizon (Figure 9). Rapid emplacement
635 of a biotite-bearing tuff on the paleosurface of the Alfisol may have led to gleization. Similar trends of
636 near-surface TOC enrichment were noted in the Entisol and Alfisol (Table 1), but these samples lacked
637 chemical ($FeO/Fe_2O_3 > 0$) and morphological evidence (drab green color) of burial gleization (Tables S5
638 and S6). Previous work on terrestrial paleosols has shown positive and significant correlations between
639 Fe^{2+} and TOC (Broz, 2020). This supports the interpretation that burial gleization, which increases Fe^{2+} in
640 bulk samples, may have been associated with the preservation of organic carbon in the surface horizon of
641 the Alfisol.

642 Organic carbon from organisms living in surface horizons of soils may have been preserved upon
643 rapid burial of the paleosurface, and therefore the trend of surface enrichment may represent the
644 preservation of endogenous organic carbon. Major losses of endogenous organic carbon from burial
645 decomposition of organic matter are common in paleosols that originally formed under oxidizing
646 conditions such as those examined here (Retallack, 2019). Despite diagenetic additions and losses of
647 organic carbon, the trend of surface enrichment of organic carbon remains apparent, even in soils that
648 formed under strongly oxidizing conditions prior to burial. These results are consistent with other studies
649 of paleosols where the surface enrichment of organic carbon was attributed to preservation of carbon from
650 organisms living above and within the soil profile (Rye and Holland, 2000; Watanabe et al., 2004;
651 Liivamägi et al., 2018; Liu et al., 2020). However, it is possible that exogenous addition of organic carbon
652 caused this enrichment, for example, by preferential groundwater flow and accumulation in the
653 paleosurface of each profile. Results from this work cannot definitively rule out groundwater as a source
654 of modern organic carbon, though it is unlikely that groundwater additions of organic carbon would have
655 preferentially accumulated in the discreet, thin (10-20 cm) surface layers of the three buried soils.

656 **3.5 Implications for Mars**

657 Recent work has considered paleosols on Mars as potential high priority environments for *in-situ*
658 biosignature investigation (Hays et al., 2017) and Mars Sample Return (Bishop et al., 2018a). This is
659 because the composition and properties of paleosols preserve evidence of paleoclimate, aqueous
660 conditions, and life (Bishop et al., 2018a). A major finding of this study is that near-surface horizons of
661 terrestrial paleosols appear to be a favorable location for SAM-EGA detection of organic carbon. Like
662 modern soils, the surface layers of Mars-analog paleosols examined here show evidence of surface
663 enrichment of organic carbon. Although the early diagenetic process of burial decomposition of organic
664 matter has likely reduced the organic carbon content of these ancient soils by at least two orders of
665 magnitude relative to modern soils (Broz, 2020), the enrichment of organic carbon in surface horizons
666 (~0.03 wt. %) and subsequent depletion in deeper layers (<0.01 wt. %) was readily observable a with
667 SAM-EGA analog instrument.

668 It should be noted that the Eocene-Oligocene (42-28 Ma) eastern Oregon paleosols are an
669 incomplete Mars analog due to several fundamental differences. Most importantly, the source of organic
670 carbon within the paleosols is primarily from microbial and/or plant biomass and represents a complex
671 consortium of life above and within the soil profile. These irrevocable differences preclude direct
672 comparisons between Earth and a presumably lifeless Mars. As such, the organic carbon component of
673 these paleosols and the resulting preservation and degradation mechanisms may not be the same on Mars,
674 but it is possible that putative paleosols at Mawrth Vallis have mineralogy analogous to terrestrial
675 paleosols and thus have a similar mineralogical control on the fate of organic carbon. Large differences in
676 age (Oligocene [33 Ma] versus Noachian [4.1-3.7 Ga]) also have implications for diagenesis. The Oregon
677 paleosols have experienced a range of minor to moderate diagenetic alteration including illitization of
678 smectite, zeolitization and celadonization all resulting from alteration to clinoptilolite facies (Retallack et
679 al., 2000; Horgan, 2016), but it is currently unclear if similar diagenetic alteration has affected potential
680 paleosol sequences on Mars. Also worth mentioning are differences in the oxidation state of the
681 atmosphere during subaerial weathering. The Oregon paleosols formed under a thoroughly oxidizing
682 atmosphere but at present the oxidation state of an early Mars atmosphere is not well constrained
683 (Ramirez et al., 2014). Leaching of Fe^{2+} in putative martian paleosols at Mawrth Vallis has been inferred
684 from spectral weathering indices, which are consistent with an anoxic, reducing atmosphere during the
685 early Noachian (Liu et al., 2021a). Lastly, there are most likely differences in the pH of fluids
686 participating in hydrolytic weathering of volcaniclastic sediments. The Oregon paleosols formed by
687 pedogenic weathering with circumneutral-pH fluids, but subaerial alteration on Mars could have preceded
688 with acidic, H_2SO_4 and HCl-rich surface waters as a result of volcanic outgassing of H_2 and SO_2 (Liu et
689 al., 2021a, 2021b). Despite these significant differences, the paleosol sequence from eastern Oregon

offers a natural example to determine if organic carbon can be detected with thermal and evolved gas analysis techniques similar to SAM-EGA.

Results from this study have implications for interpreting the chemical and isotopic biosignature preservation potential of Al and Fe smectite-bearing weathering profiles on Mars. Observations of refractory organic compounds that persist in terrestrial paleosols with Mars-like mineralogy provide a reference frame for interpreting future observations of putative weathering profiles on Mars. It is possible that clay minerals and/or amorphous phases in martian weathering profiles have imparted a similar control on the fate of organic carbon. However, putative martian weathering profiles have likely been subject to both galactic cosmic ray bombardment and the accumulation of oxychlorine salts that, together, have likely contributed to the degradation of organic matter in the top 1-2 m of the martian surface (Dartnell et al., 2007; Freissinet et al., 2015). This poses major challenges for the future detection of organic carbon in martian weathering profiles using current drilling techniques. Trace amounts of organic carbon may have been preserved in the Oregon paleosols (Table 2), but if putative martian paleosols have a Cretaceous exposure age comparable with Gale crater sedimentary rocks (Farley et al., 2013), millions of years of cosmic ray bombardment and interactions with oxychlorine salts may have led to the oxidation of a significant fraction of the organic carbon pool.

This work also provides an initial framework for investigation and sampling of martian weathering profiles should they be encountered by current or future landed missions. If possible, future *in-situ* analysis of putative weathering profiles should begin at the apparent ancient surface horizon (e.g., the buried topsoil layer) and sample down section into the unaltered protolith, similar to the sampling of a terrestrial soil profile. If the entire profile is not accessible for investigation (e.g., outcrop is at a topographic position inaccessible to the rover), the near-surface horizons of the profile, just below the overlying burial layer, should be considered the highest priority target for remote sensing, contact science, and collection of a drilled sample for sample return to Earth. Two locations on Mars where current and future landed missions could encounter a paleosol profile are discussed below.

Mawrth Vallis

Previous work identified compositional and morphological similarities between the eastern Oregon paleosol sequence and layered outcrops at Mawrth Vallis (Horgan et al., 2012; Hays et al., 2017; Lantz et al., 2020; Smith and Horgan, 2021). The compositional stratigraphy at Mawrth Vallis has been interpreted as a paleosol sequence (Horgan et al., 2012) or a deep weathering profile (Liu et al., 2021a). Here, a ~200 m stack of layered sedimentary rocks has spectral signatures consistent with pedogenic-like alteration of mafic sediments (Horgan, 2013). The basal Fe/Mg smectite unit at Mawrth Vallis is dominated by spectral signatures of Fe/Mg smectite and is consistent with subaerial alteration under a

warm and wet climate (Loizeau et al., 2015; Poulet et al., 2020). This basal unit transitions upward into a thin, ferrous-bearing clay unit that could have resulted from reducing conditions during subaerial weathering. This unit is overlain by layered rocks containing minerals consistent with formation in acidic and evaporitic geochemical settings, inferred from spectral signatures consistent with mixtures of smectite and jarosite (the "doublet' spectral feature) (Noe Dobrea et al., 2016; Danielson et al., 2019; Bishop et al., 2020) . Stratigraphically higher, layered rocks with signatures of Al and Fe smectite are consistent with pedogenic weathering of volcaniclastic sediments under a semi-arid climate. Finally, the uppermost layers are characterized by accumulations of poorly crystalline aluminosilicates, suggesting minimal or cool-climate alteration, which may represent the terminus of warm and wet conditions on early Mars (Bishop et al., 2020). The entire sequence is then capped by dark-toned sands and/or lava flows. One hypothesis to explain the stratigraphy at Mawrth Vallis is that it may represent the cooling and drying of the Martian climate during the mid to late Noachian (Bishop and Rampe, 2016; Bishop et al., 2020). Similarly, the Oregon paleosol sequence represents a transition from warm and wet conditions. The intensely weathered basal Clarno Formation paleosols transition upward into less-weathered semi-arid paleosols of the middle Big Basin Member, which contains both oxidized (red, brown) and reduced (yellow, black) paleosols (Figure 1). These are subsequently overlain by minimally weathered paleosols of the Oligocene Turtle Cove Member with accumulations of unweathered volcanic glass, amorphous colloids, calcite and hydrated silica, which are thought to represent the terminus of warm and wet climate conditions in eastern Oregon. Terrestrial paleosols at the analog site have therefore been considered analogous to dioctahedral clay sequences on Mars. The layered stratigraphy at Mawrth Vallis currently stand as the best example of a putative paleosol sequence on Mars, but other locations, such as Jezero Crater, also show VNIR spectra consistent with subaerial alteration of mafic sediments.

Jezero Crater

Spectral signatures of Al-bearing clay minerals and/or silica deposits that could have formed in subaerial environments were detected approximately 3 km from the Perseverance rover landing site at Jezero Crater. Across Jezero's western delta and northern fans, there are strong and ubiquitous orbital detections of Al-bearing clay minerals and/or silica that could be either detrital or authigenic in origin (Horgan et al., 2020). The strongest signatures across the western delta are associated with features that resemble point bar deposits and are consistent with formation in subaerial and/or seasonally waterlogged paleoenvironments (Horgan et al., 2020). If authigenic in origin, these deposits could be subaerial paleoenvironments and include individual paleosol profiles. If targeted for *in-situ* examination by *Perseverance* rover, these deposits could provide

757 critical information about the climate and duration of delta activity at Jezero Crater (Horgan et
758 al., 2020).

759 **Conclusions**

760 The objectives of this study were a) to determine whether the organic carbon content of ~33-
761 million-year-old paleosols can be detected with a thermal and evolved gas analyzer configured to operate
762 like the SAM-EGA instrument onboard *Curiosity* Mars rover, and b) use radiocarbon (^{14}C) dating to
763 constrain the age of organic carbon in bulk paleosol samples. Radiocarbon dating of organic carbon in
764 four paleosol samples revealed the presence of recent and/or modern exogenous organic carbon. Samples
765 from 10 - 20 cm were dated to ~6,200 years BP and had a fraction modern (FM) value of ~0.4, while a
766 single deeper sample collected from 43 cm into the outcrop had a radiocarbon age of ~14,600 years BP
767 and ~0.16 fM. The presence of radiocarbon in paleosols could have resulted from the addition of small
768 amounts of modern organic carbon that mixed with ^{14}C-free endogenous organic carbon. Alternatively, a
769 diagenetic event between 6-14 Ka could have introduced exogenous organics, possibly through
770 groundwater alteration and/or precipitation-driven leaching of dissolved organic carbon. Application of a
771 two-endmember mixing model (Equation 1) to the $D^{14}C$ values of bulk samples values provided
772 supporting evidence for the hypothesis that paleosols from the site contain small amounts of modern
773 organic carbon. The amount of modern carbon ($D^{14}C$= 0‰) that could have been added to a pool of
774 Oligocene-age carbon ($D^{14}C$ = -999‰) was determined to range from ~0.5 – 3% of the total carbon in
775 each sample. These results highlight a new approach for constraining the age and sources of organic
776 matter in terrestrial paleosols.

777 SAM-EGA-like characterization of paleosols showed evolutions of CO, NO, CO_2, and organic
778 fragments. Coevolutions of CO_2 and organic fragments at ~400° C suggested the presence of refractory
779 organic carbon. However, like other oxidized terrestrial paleosols of Cenozoic age and older, only trace
780 amounts (<0.1 wt. %) of organic carbon was detected, which most likely was a result of diagenetic
781 decomposition of organic matter over geological time scales. Many samples examined in this work
782 typically contained very low amounts (~0.01 wt. %) of organic carbon, but these low values were
783 nevertheless detectable by SAM-like evolved gas analysis of bulk samples. These results suggest the
784 organic fraction of potential martian weathering profiles may be detectable with evolved gas analysis,
785 even if organic concentrations are low.

786 A major result of this work was that organic carbon was concentrated in near-surface horizons of
787 paleosols while deeper horizons were depleted in organic carbon. Like modern soils, these ancient soils
788 were enriched in organic carbon in near-surface horizons, and it appears that this trend persisted in these
789 samples despite burial decomposition of organic carbon over geological time scales. Alternatively,

790 modern carbon could have leached into the outcrop, but it is unlikely such organic contamination would
791 preferentially accumulate in the surface layers of each successive buried soil profile. Enrichment of
792 organic carbon in the original surface horizons of buried weathering profiles on Mars may therefore
793 constitute a putative chemical biosignature. This work demonstrates that analytical techniques similar to
794 SAM-EGA can detect trace amounts of organic carbon in complex pedogenic mineral matrices. The
795 search for past life on ancient land surfaces of Mars should include targeting Martian weathering profiles
796 for *in-situ* biosignature investigation and Mars Sample Return.
797

798 ## Additional Information

799

800 **Acknowledgements**

801 This work was performed on and adjacent to the ancestral homelands of the Numu, Cayuse, Umatilla,
802 Walla Walla, and Confederated Tribes of the Warm Springs who were present before western settlement.
803 Many thanks to Elizabeth Rampe and Paul Niles for the opportunity to work on this project and for
804 providing research direction during a summer internship. This work was completed as part of a PhD
805 dissertation supervised by Greg Retallack and Lucas C.R. Silva. Xiaomei Xu performed radiocarbon
806 dating and data interpretation, both of which were integral to this work. Megan Barrington and Barry
807 Hughes assisted with fieldwork and entertained thoughtful discussion. Anais Roussel, Angela Olsen,
808 Marshall Styczinski, Paul Regensberger and Joe Caggiano reviewed early versions of the manuscript.
809 Funding to A.P.B. from the National Science Foundation, Geological Society of America, The Clay
810 Minerals Society, The Society of Sedimentary Geology, and the Central Oregon Geoscience Society
811 aided in the completion of this project.
812

813 **Author Contribution Statement**

814 A.P.B and J.V.C designed the study, performed all laboratory analyses and drafted the manuscript. J.V.C,
815 D.W.M, P.D.A, and B.S contributed to data analysis and interpretation. B.H.H identified similarities
816 between Mars and Oregon paleosols and assisted with fieldwork and data interpretation. L.C.R.S
817 provided radiocarbon analyses and interpreted the data. J.V.C, P.D.A, B.S, D.W.M, and L.C.R.S
818 supervised the project. A.P.B drafted all figures. All authors contributed to the manuscript.
819

820 **Author Disclosure Statement**

821 No competing financial interests exist.

822 **Data Availability Statement**

All data supporting the conclusions can be found within the article and in the following repository: Broz, 2022. All raw data to reproduce EGA traces are included in the supplementary dataset (Broz, 2022).

4 References

Alekseeva, T. V, Zolotareva, B.N., and Kolyagin, Y.G., 2019, Nonhydrolyzable Part of Soil Organic Matter in Buried and Modern Soils: Eurasian Soil Science, v. 52, p. 632–643, doi:10.1134/S1064229319060024.

Amundson, R., 2018, Meteoric water alteration of soil and landscapes at Meridiani Planum, Mars: Earth and Planetary Science Letters, v. 488, p. 155–167, doi:10.1016/j.epsl.2018.02.012.

Apesteguia, M., Plante, A.F., and Virto, I., 2018, Methods assessment for organic and inorganic carbon quantification in calcareous soils of the Mediterranean region: Geoderma Regional, v. 12, p. 39–48, doi:10.1016/j.geodrs.2017.12.001.

Archer, P.. et al., 2014, Abundances and implications of volatile-bearing species from evolved gas analysis of the Rocknest aeolian deposit, Gale Crater, Mars: Journal of Geophysical Research : Planets, p. 237–254, doi:10.1002/2013JE004493.Received.

Beaty, D.W., Grady, M.M., Mcsween, H.Y., Sefton-Nash, E., Carrier, B.., Altieri, F., and Al., E., 2019, The potential science and engineering value of samples delivered to Earth by Mars sample return: Meteoritics & Planetary Science, v. 671, p. 667–671, doi:10.1111/maps.13232.

Bestland, E.., 1997, Alluvial Terraces and Paleosols As Indicators Of Early Oligocene Climate Change (John-Day Formation, Oregon): Journal Of Sedimentary Research, v. 67, p. 840–855, doi:10.1306/D4268653-2B26-11D7-8648000102C1865D.

Bestland, E.A., 2002, Fossil Andisols identified with mass-balance geochemistry (Oligocene John Day Formation, Oregon, U.S.A.): Journal of Sedimentary Research, v. 72, p. 673–686, doi:10.1306/021802720673.

Bishop, J.L. et al., 2018a, Potential high priority subaerial environments for Mars sample return: Proceedings of the Second International Mars Sample Return Conference, v. 2071, doi:2018LPICo2071.6043I.

Bishop, J.L., Fairén, A.G., Michalski, J.R., Gago-duport, L., Baker, L.L., Velbel, M.A., Gross, C., and Rampe, E.B., 2018b, Surface clay formation during short-term warmer and wetter conditions on a largely cold ancient Mars: Nature Astronomy, v. 2, p. 206–213, doi:10.1038/s41550-017-0377-9.

Bishop, J.L., Gross, C., Danielsen, J., Parente, M., Murchie, S.L., Horgan, B., Wray, J.J., Viviano, C., and Seelos, F.P., 2020, Multiple mineral horizons in layered outcrops at Mawrth Vallis, Mars, signify changing geochemical environments on early Mars: Icarus, v. 341, p. 113634, doi:10.1016/j.icarus.2020.113634.

Bishop, J.L., Loizeau, D., Mckeown, N.K., Saper, L., Dyar, M.D., Des, D.J., Parente, M., and Murchie, S.L., 2013, What the ancient phyllosilicates at Mawrth Vallis can tell us about possible habitability on early Mars: Planetary and Space Science, v. 86, p. 130–149,

doi:10.1016/j.pss.2013.05.006.

Bishop, J.L., and Rampe, E.B., 2016, Evidence for a changing Martian climate from the mineralogy at Mawrth Vallis: Earth and Planetary Science Letters, v. 448, p. 42–48, doi:10.1016/j.epsl.2016.04.031.

Broz, A.P., 2022, Detection of organic carbon in Mars-analog paleosols with thermal and evolved gas analysis [Data set]: Mendelay, doi:10.17632/bkvcff9dw8.1.

Broz, A.P., 2020, Organic Matter Preservation in Ancient Soils of Earth and Mars: Life, v. 10, doi:doi:10.3390/life10070113.

Broz, A.P., Clark, J.V., Archer, P.., Sutter, B., Tu, V.M., Silva, L.C.R., and Horgan, B.H.N., 2021, Radiocarbon dating of Mars-analog paleosols reveals contamination with exogenous organic carbon, *in* Terrestrial Analogs, v. 8094.

Broz, A.P., Clark, J., Sutter, B., Ming, D.W., Tu, V., Horgan, B., and Silva, L.C.R., 2022, Mineralogy and diagenesis of Mars-analog paleosols from eastern Oregon, USA: Icarus, v. 380, p. 114965, doi:10.1016/j.icarus.2022.114965.

Cannon, K.M., Sutter, B., Ming, D.W., Boynton, W. V., and Quinn, R., 2012, Perchlorate induced low temperature carbonate decomposition in the Mars Phoenix Thermal and Evolved Gas Analyzer (TEGA): Geophysical Research Letters, v. 39, p. 2–6, doi:10.1029/2012GL051952.

Carter, J., Loizeau, D., Mangold, N., Poulet, F., and Bibring, J., 2015, Widespread surface weathering on early Mars : A case for a warmer and wetter climate: Icarus, v. 248, p. 373–382, doi:10.1016/j.icarus.2014.11.011.

Danielson, J.., Bishop, J.., Usabel, G.S., Miura, J.., Sessa, A.., Wray, J.., Itoh, Y., Parente, M., and Murchie, S.., 2019, Characterization of outcrops containing “doublet” spectra at Mawrth Vallis, Mars: Lunar and Planetary Science Conference, v. 2019, p. 1–179, doi:10.1029/2008g.

Dartnell, L.R., Desorgher, L., Ward, J.M., and Coates, A.J., 2007, Martian sub-surface ionising radiation : biosignatures and geology ∗: Biogeosciences, v. 4, p. 545–558.

Dynarski, K.A., Bossio, D.A., and Scow, K.M., 2020, Dynamic Stability of Soil Carbon: Reassessing the “Permanence” of Soil Carbon Sequestration: Frontiers in Environmental Science, v. 8, doi:10.3389/fenvs.2020.514701.

Eigenbrode, J.L. et al., 2018, Organic matter preserved in 3-billion-year-old mudstones at Gale crater, Mars: Science, v. 360, p. 1096–1101, doi:10.1126/science.aas9185.

Farley, K.A., Malespin, C., Mahaffy, P., and Grotzinger, J.P., 2013, In Situ Radiometric and Exposure Age Dating of the Martian Surface — Supplementary Materials: Science Express, p. 1–9, doi:10.1126/science.1247166.

Fernández, J.M., Peltre, C., Craine, J.M., and Plante, A.F., 2012, Improved characterization of soil organic matter by thermal analysis using CO2/H2O evolved gas analysis: Environmental Science and Technology, v. 46, p. 8921–8927, doi:10.1021/es301375d.

Fornaro, T., Steele, A., and Brucato, J.R., 2018, Catalytic/protective properties of martian minerals and implications for possible origin of life on mars: Life, v. 8, p. 1–41, doi:10.3390/life8040056.

François, P., Szopa, C., Buch, A., Coll, P., Mcadam, A.C., Mahaffy, P.R., Freissinet, C., Glavin, D.P., and Cabane, M., 2015, Magnesium sulfate as a key mineral for the detection of organic molecules on Mars using pyrolysis: Journal of Geophysical Research – Planets, p. 61–74, doi:10.1002/2015JE004884.Received.

Freissinet, C. et al., 2015, Organic molecules in the Sheepbed Mudstone, Gale Crater, Mars: Journal of Geophysical Research : Planets, v. 120, p. 495–514, doi:10.1002/2014JE004737.Received.

Fremd, T.J., 1996, Data Quality in Terrestrial Assemblages: Perspectives from Volcaniclastic Sequences of the John Day Basin, Oregon: The Paleontological Society Special Publications, v. 8, p. 131–131, doi:10.1017/s2475262200001337.

Guggenberger, G., and Kaiser, K., 2003, Dissolved organic matter in soil : challenging the paradigm of sorptive preservation: Geoderma, v. 113, p. 293–310, doi:10.1016/S0016-7061(02)00366-X.

Hays, L.E., Graham, H. V., Des Marais, D.J., Hausrath, E.M., Horgan, B., McCollom, T.M., Parenteau, M.N., Potter-McIntyre, S.L., Williams, A.J., and Lynch, K.L., 2017, Biosignature Preservation and Detection in Mars Analog Environments: Astrobiology, v. 17, p. 363–400, doi:10.1089/ast.2016.1627.

Horgan, B.H.N., 2013, Climate change and a sequence of habitable ancient surface environments preserved in pedogenically altered sediments at Mawrth Vallis, Mars., *in* Lunar and Planetary Science Conference, p. 3059.

Horgan, B., 2016, Strategies for Searching for Biosignatures in Ancient Martian Sub-Aerial Surface Environments: Biosignature Preservation and Detection in Mars Analog Environments, p. 7463, doi:10.1089/ast.2016.1627.

Horgan, B.H.N., Anderson, R.B., Dromart, G., Amador, E.S., and Rice, M.S., 2020, The mineral diversity of Jezero crater : Evidence for possible lacustrine carbonates on Mars: Icarus, v. 339, p. 113526, doi:10.1016/j.icarus.2019.113526.

Horgan, B., Bishop, L., Christensen, P.R., and Bell, J.F., 2012, Potential ancient soils preserved at Mawrth Vallis from comparisons with Eastern Oregon paleosols: Implications for Early Martian Climate: Third Conference on Early Mars, v. 7074, p. 12–13.

Horgan, B., Rutledge, A., and Rampe, E.., 2018, Clay mineralogy and crystallinity as a climatic indicator: Evidence for both cold and temperate conditons on early Mars: 46th Lunar and Planetary Science Conference, p. 3–4, doi:10.1029/2006.

Ivanov, M.A., Slyuta, E.N., Grishakina, E.A., and Dmitrovskii, A.A., 2020, Geomorphological Analysis of ExoMars Candidate Landing Site Oxia Planum: Solar System Research, v. 54, p. 1–14, doi:10.1134/S0038094620010050.

Kleber, M., Bourg, I.C., Coward, E.K., Hansel, C.M., Myneni, S.C.B., and Nunan, N., 2021, Dynamic interactions at the mineral–organic matter interface: Nature Reviews Earth and Environment, v. 2, p. 402–421, doi:10.1038/s43017-021-00162-y.

Kleber, M., Mikutta, R., Torn, M.., and Jahn, R., 2005, Poorly crystalline mineral phases protect organic matter in acid subsoil horizons: European Journal of Soil Science, p. 717–725, doi:10.1111/j.1365-2389.2005.00706.x.

Kremer, B., Kaźmierczak, J., and Środoń, J., 2017, Cyanobacterial-algal crusts from Late

947 Ediacaran paleosols of the East European Craton: Precambrian Research,
948 doi:10.1016/j.precamres.2017.12.018.

949 Krull, E.S., and Retallack, G.J., 2000, 13C depth profiles from paleosols across the Permian-
950 Triassic boundary : Evidence for methane release: GSA Bulletin, v. 112, p. 1459–1472.

951 Kurth, V.J., MacKenzie, M.D., and DeLuca, T.H., 2006, Estimating charcoal content in forest
952 mineral soils: Geoderma, v. 137, p. 135–139, doi:10.1016/j.geoderma.2006.08.003.

953 De la Rosa, J.M., González-Pérez, J.A., González-Vázquez, R., Knicker, H., López-Capel, E.,
954 Manning, D.A.C., and González-Vila, F.J., 2008, Use of pyrolysis/GC-MS combined with
955 thermal analysis to monitor C and N changes in soil organic matter from a Mediterranean
956 fire affected forest: Catena, v. 74, p. 296–303, doi:10.1016/j.catena.2008.03.004.

957 Lantz, C., Poulet, F., Loizeau, D., Riu, L., Pilorget, C., Carter, J., Dypvik, H., Rull, F., and
958 Werner, S.C., 2020, Planetary Terrestrial Analogues Library project: 1. characterization of
959 samples by near-infrared point spectrometer: Planetary and Space Science, v. 189, p.
960 104989, doi:10.1016/j.pss.2020.104989.

961 Lehmann, J., and Kleber, M., 2015, The contentious nature of soil organic matter: Nature, p. 1–9,
962 doi:10.1038/nature16069.

963 Lewis, J.M.T. et al., 2021, Pyrolysis of Oxalate, Acetate, and Perchlorate Mixtures and the
964 Implications for Organic Salts on Mars: Journal of Geophysical Research: Planets, v. 126,
965 doi:10.1029/2020JE006803.

966 Liivamägi, S., Rodoń, J., Bojanowski, M., Gerdes, A., Stanek, J.J., Williams, L., and Szczerba,
967 M., 2018, Paleosols on the Ediacaran basalts of the East European Craton: a unique record
968 of paleoweathering with minimum diagenetic overprint: Precambrian Research,
969 doi:10.1016/j.precamres.2018.07.020.

970 Liu, J., He, H., Michalski, J., Cuadros, J., Yao, Y., Tan, W., Qin, X., Li, S., and Wei, G., 2020,
971 Reflectance spectroscopy applied to clay mineralogy and alteration intensity of a thick
972 basaltic weathering sequence in Hainan Island , South China: Applied Clay Science, p.
973 105923, doi:10.1016/j.clay.2020.105923.

974 Liu, J., Michalski, J.R., Tan, W., He, H., Ye, B., and Xiao, L., 2021a, Anoxic chemical
975 weathering under a reducing greenhouse on early Mars: Nature Astronomy,
976 doi:https://doi.org/10.1038/s41550-021-01303-5.

977 Liu, J., Michalski, J.R., and Zhou, M., 2021b, Intense subaerial weathering of eolian sediments
978 in Gale crater, Mars: Science Advances, v. 7, doi:DOI: 10.1126/sciadv.abh2687.

979 Loizeau, D. et al., 2020, ExoMars 2020 Surface Mission: Choosoing a Landing Site: v. 2019, p.
980 2019–2020.

981 Loizeau, D., Mangold, N., Poulet, F., Bibring, J., Bishop, J.L., Michalski, J., and Quantin, C.,
982 2015, History of the clay-rich unit at Mawrth Vallis, Mars: High- resolution mapping of a
983 candidate landing site: Journal of Geophysical Research: Planets, p. 1820–1846,
984 doi:10.1002/2015JE004894.Received.

985 Loizeau, D., Quantin-nataf, C., Carter, J., Flahaut, J., Thollot, P., Lozac, L., and Millot, C., 2018,
986 Quantifying widespread aqueous surface weathering on Mars : The plateaus south of
987 Coprates Chasma: Icarus, v. 302, p. 451–469, doi:10.1016/j.icarus.2017.11.002.

Mahaffy, P.R. et al., 2012, The sample analysis at mars investigation and instrument suite: Space Science Reviews, v. 170, p. 401–478, doi:10.1007/s11214-012-9879-z.

Marin-Spiotta, E., Chaopricha, N.T., Plante, A.F., Diefendorf, A.F., Mueller, C.W., Grandy, A.S., and Mason, J.A., 2014, Long-term stabilization of deep soil carbon by fire and burial during early Holocene climate change: Nature Geoscience, v. 7, p. 428–432, doi:10.1038/ngeo2169.

Matthewman, R., Cotton, L.J., Martins, Z., and Sephton, M.A., 2012, Organic geochemistry of late Jurassic paleosols (Dirt Beds) of Dorset , UK: Marine and Petroleum Geology, v. 37, p. 41–52, doi:10.1016/j.marpetgeo.2012.05.009.

Mcadam, A.., Sutter, B., Archer, P.., Franz, H.., and Eigenbrode, J.., 2020a, The chemistry and mineralogy of the Glen Torridon clay-bearing unit from Mars Science Laboratory Sample Analysis at Mars: 51st Lunar and Planetary Science Conference, v. 2243, p. 60–74.

Mcadam, A.C., Sutter, B., Archer, P.D., Franz, H.B., Wong, G.M., Lewis, J.M.T., Eigenbrode, J.L., and Stern, J.C., 2020b, Constraints on the Mineralogy and Geochemistry of Vera Rubin Ridge , Gale Crater , Mars , From Mars Science Laboratory Sample Analysis at Mars Evolved Gas Analyses: Journal of Geophysical Research : Planets, p. 1–26, doi:10.1029/2019JE006309.

Miller, K.B., McCahon, T.J., and West, R.R., 1996, Lower Permian (wolfcampian) paleosol-bearing cycles of the U.S. Midcontinent: Evidence of climatic cyclicity: Journal of Sedimentary Research, v. 66, p. 71–84, doi:10.1306/D42682B6-2B26-11D7-8648000102C1865D.

Ming, D.W. et al., 2014, Volatile and Organic Compositions of Sedimentary Rocks in Yellowknife Bay , Gale Crater , Mars: Science Express, p. 1–15, doi:10.1126/science.1245267.

Navarro-González, R., Iñiguez, E., De La Rosa, J., and McKay, C.P., 2009, Characterization of organics, microorganisms, desert soils, and mars-like soils by thermal volatilization coupled to mass spectrometry and their implications for the search for organics on mars by phoenix and future space missions: Astrobiology, v. 9, p. 703–715, doi:10.1089/ast.2008.0284.

Noe Dobrea, E.Z., McAdam, A.C., Freissinet, C., Franz, H., Belmahdi, I., Hammersley, M.R., and Stoker, C.R., 2016, Characterizing the mechanisms for the preservation of organics at the Painted Desert: Lessons for MSL, Exo-Mars, and Mars 2020: 47th Lunar and Planetary Science Conference, p. Abstract #2796.

PiPujol, M.D., and Buurman, P., 1994, The distinction between ground-water gley and surface-water gley phenomena in Tertiary paleosols of the Ebro basin, NE Spain: Palaeogeography, Palaeoclimatology, Palaeoecology, v. 110, p. 103–113, doi:10.1016/0031-0182(94)90112-0.

Plante, A.F., Fernández, J.M., Haddix, M.L., Steinweg, J.M., and Conant, R.T., 2011, Biological, chemical and thermal indices of soil organic matter stability in four grassland soils: Soil Biology and Biochemistry, v. 43, p. 1051–1058, doi:10.1016/j.soilbio.2011.01.024.

Poulet, F., Gross, C., Horgan, B., Loizeau, D., Bishop, J.L., Carter, J., and Orgel, C., 2020, Mawrth Vallis, Mars: A Fascinating Place for Future In Situ Exploration: Astrobiology, v. 20, p. 1–36, doi:10.1089/ast.2019.2074.

Ramirez, R.M., Kopparapu, R., Zugger, M.E., Robinson, T.D., Freedman, R., and Kasting, J.F.,

2014, Warming early Mars with CO2 and H2: Nature Geoscience, v. 7, p. 59–63, doi:10.1038/ngeo2000.

Rampe, E.., Morris, R. V, Ruff, S.W., Dehouck, E., Achilles, C.N., Ming, D.W., Bish, D.L., and Chipera, S.J., 2014, Amorphous phases on the surface of Mars: Eighth International Conference on Mars, p. 1–2.

Raynaud, X., and Nunan, N., 2014, Spatial ecology of bacteria at the microscale in soil: PLoS ONE, v. 9, doi:10.1371/journal.pone.0087217.

Reardon, P.N., Chacon, S.S., Walter, E.D., Bowden, M.E., Washton, N.M., and Kleber, M., 2016, Abiotic Protein Fragmentation by Manganese Oxide: Implications for a Mechanism to Supply Soil Biota with Oligopeptides: Environmental Science and Technology, v. 50, p. 3486–3493, doi:10.1021/acs.est.5b04622.

Retallack, G.J., 2014, Paleosols and paleoenvironments of early Mars: Geology, v. 42, p. 755–758, doi:10.1130/G35912.1.

Retallack, G.J., 2019, Soil of the Past: Wiley Blackwell.

Retallack, G.J., Bestland, E.., and Fremd, T.., 2000, Eocene and Oligocene Paleosols of Central Oregon: Geological Society of America Special Paper, v. 344, p. 1–192, doi:10.1046/j.1365-3091.2001.0394c.x.

Retallack, G.J., and Krull, E.S., 1999, Landscape ecological shift at the Permian – Triassic boundary in Antarctica: Australian Journal of Earth Sciences, v. 46, p. 785–812.

Retallack, G.J., and Mao, X., 2019, Paleoproterozoic (ca . 1 . 9 Ga) megascopic life on land in Western Australia: Palaeogeography, Palaeoclimatology, Palaeoecology, v. 532, p. 109266, doi:10.1016/j.palaeo.2019.109266.

Retallack, G.J., Wynn, J.G., and Fremd, T.J., 2004, Glacial-interglacial-scale paleoclimatic change without large ice sheets in the Oligocene of central Oregon: Geology, v. 32, p. 297–300, doi:10.1130/G20247.1.

Rye, R., and Holland, H., 2000, Life associated with a 2 . 76 Ga ephemeral pond ?: Evidence from Mount Roe # 2 paleosol: Geology, v. 28, p. 483–486, doi:10.1130/0091-7613(2000)28<483:LAWAGE>2.0.CO;2.

Schmidt, M.W.I. et al., 2011, Persistence of soil organic matter as an ecosystem property: Nature, doi:10.1038/nature10386.

Sheldon, N.D., Retallack, G.J., and Tanaka, S., 2002, Geochemical Climofunctions from North American Soils and Application to Paleosols across the Eocene - Oligocene Boundary in Oregon Geochemical Climofunctions from North American Soils and Application to Paleosols across the Eocene-Oligocene Boundary in Or: The Journal of Geology, v. 110, p. 687–696, doi:10.1086/342865.

Sickman, J.O., DiGiorgio, C.L., Davisson, M.L., Lucero, D.M., and Bergamaschi, B., 2010, Identifying sources of dissolved organic carbon in agriculturally dominated rivers using radiocarbon age dating: Sacramento-San Joaquin River Basin, California: Biogeochemistry, v. 99, p. 79–96, doi:10.1007/s10533-009-9391-z.

Silva, L.C.R., Corrêa, R.S., Doane, T.A., Pereira, E.I.P., Horwath, W.R., Silva, L.C.R., Corrêa, R.S., Doane, T.A., and Pereira, E.I.P., 2013, Unprecedented carbon accumulation in mined

soils : the synergistic effect of resource input and plant species invasion: Ecological Applications, v. 23, p. 1345–1356, doi:10.1890/12-1957.1.

Smith, R.., and Horgan, B.H.N., 2021, Nanoscale Variations in Natural Amorphous and Nanocrystalline Weathering Products in Mafic to Intermediate Volcanic Terrains on Earth : Implications for Amorphous Detections on Mars: Journal of Geophysical Research: Planets, v. 126, p. 1–30, doi:10.1029/2020JE006769.

Smith, R.., Horgan, B., Rampe, E., and Dehouck, E., 2018a, The Composition of Amorphous Phases in Soils and Sediments on Earth and Mars: 49th Lunar and Planetary Science Conference 2018, p. 14–15.

Smith, R.J., Rampe, E.B., Horgan, B.H.N., and Dehouck, E., 2018b, Deriving Amorphous Component Abundance and Composition of Rocks and Sediments on Earth and Mars: Journal of Geophysical Research: Planets, v. 123, p. 2485–2505, doi:10.1029/2018JE005612.

Stern, J.C., Sutter, B., Freissinet, C., Navarro-González, R., Mckay, C.., and Archer, P.D., 2015, Evidence for indigenous nitrogen in sedimentary and aeolian deposits from the Curiosity rover investigations at Gale ...: PNAS, doi:10.1073/pnas.1420932112.

Sutter, B., Boynton, W. V., Ming, D.W., Niles, P.B., Morris, R. V., Golden, D.C., Lauer, H. V., Fellows, C., Hamara, D.K., and Mertzman, S.A., 2012, The detection of carbonate in the martian soil at the Phoenix Landing site: A laboratory investigation and comparison with the Thermal and Evolved Gas Analyzer (TEGA) data: Icarus, v. 218, p. 290–296, doi:10.1016/j.icarus.2011.12.002.

Sutter, B., Mcadam, A.., Mahaffy, P.., Ming, D.., Edgett, K.., Rampe, E.., Eigenbrode, J.., Franz, H.., and Freissinet, C., 2017, Evolved gas analyses of sedimentary rocks and eolian sediment in Gale Crater, Mars: Results of the Curiosity rover's sample analysis at Mars instrument from Yellowknife Bay to the Namib Dune: Journal of Geophysical Research : Planets, p. 2574–2609, doi:10.1002/2016JE005225.

Sweeney, K.E., Roering, J.J., and Ellis, C., 2015, Experimental evidence for hillslope control of landscape scale: Science, v. 349, p. 51–53, doi:10.1126/science.aab0017.

Szopa, C. et al., 2020, First Detections of Dichlorobenzene Isomers and Trichloromethylpropane from Organic Matter Indigenous to Mars Mudstone in Gale Crater , Mars : Results from the Sample Analysis at Mars Instrument Onboard the Curiosity Rover: v. 20, p. 292–306, doi:10.1089/ast.2018.1908.

Viviano-Beck, C.E. et al., 2014, Revised CRISM spectral parameters and summary products based on the currently detected mineral diversity on Mars: Journal of Geophysical Research: Planets, v. 119, p. 1403–1431, doi:10.1002/2014JE004627.

Watanabe, Y., Martin, J.E.., and Ohmoto, H., 2000, Geochemical evidence for terrestrial ecosystems 2.6 billion years ago: Nature, v. 408, doi:10.1038/35046052.

Watanabe, Y., Stewart, B.W., and Ohmoto, H., 2004, Organic- and carbonate-rich soil formation ~2.6 billion years ago at Schagen, East Transvaal district, South Africa: Geochimica et Cosmochimica Acta, v. 68, p. 2129–2151, doi:10.1016/j.gca.2003.10.036.

Ye, B., and Michalski, J.R., 2021, Precipitation-Driven Pedogenic Weathering of Volcaniclastics on Early Mars: Geophysical Research Letters, v. 48, p. 1–10, doi:10.1029/2020GL091551.

1113 Zech, M., Kreutzer, S., Zech, R., Goslar, T., Meszner, S., Mcintyre, C., Häggi, C., Eglinton, T.,
1114 Faust, D., and Fuchs, M., 2017, Comparative 14C and OSL dating of loess-paleosol
1115 sequences to evaluate post-depositional contamination of n-alkane biomarkers: Quaternary
1116 Research, v. 87, p. 180–189, doi:10.1017/qua.2016.7.
1117
1118